Figure 4
EPO promotes angiogenesis in infarcted hearts. (**A**) Double immunostaining for PECAM (green) and dystrophin (brown) in the border area (MI group) or LV free wall (sham group) of EPO- and saline-treated (control) hearts. Scale bars: 20 μm. The number of vessels and the ratio of vessels to cardiomyocyte were measured ($n = 8$ for each). $^*P < 0.05$; $^\#P < 0.01$. (**B**) Double immunohistochemical staining for α SMA (green) and PECAM (red) shown together with TO-PRO-3 (blue) staining in the border area (MI group) or LV free wall (sham group) 14 days after operation. The number of α-SMA–positive vessels in the ischemic area was determined ($n = 8$). Scale bars: 100 μm. $^*P < 0.05$. (**C**) Coronary flow was measured in EPO- and saline-treated (control) hearts 14 days after MI with or without sodium nitroprusside (SNP, 10^{-4} M) ($n = 6$). $^*P < 0.05$. (**D**) Representative images of hypoxyprobe staining (brown) of EPO- and saline-treated (control) hearts in the border area (MI group) or LV free wall (sham group) 7 days after operation. The rate of hypoxyprobe-positive area in the border area was measured ($n = 3$). Scale bars: 500 μm (thick bars); 100 μm (thin bars). $^*P < 0.01$.

showed that EPO-induced antiapoptotic effects were abolished by transducing adenoviral vectors, which encode the dominant negative form of EPOR (Figure 3E). These results suggest that EPO accomplishes antiapoptotic effects on cardiomyocytes through the EPO/EPOR signaling pathways. EPO has been reported to activate several kinases including Akt and ERK, which promote cell surviving pathways (10, 19). We thus determined whether EPO inhibits the death of cardiomyocytes by activating these kinases. Indeed, both Akt and ERK were activated in cultured cardiomyocytes by EPO in a time- and dose-dependent manner, and these activations were abolished by transducing dominant negative EPOR (Supplemental Figure 2, A–C). Inhibitions of Akt and ERK using respective kinase inhibitors suppressed EPO-induced reduction in the number of TUNEL-positive cardiomyocytes and EPO-induced downregulation of cleaved caspase-3 (Supplemental Figure 2, D and E), suggesting that EPO prevents apoptotic death of cardiomyocytes at least in part by activating Akt and ERK through the EPO/EPOR system in cardiomyocytes.

Angiogenic cytokines mediate EPO-induced cardioprotection. To determine the angiogenic effects of EPO, we performed immunohistochemical double-staining of infarcted hearts for PECAM and dystrophin. EPO treatment markedly increased the number of PECAM-positive capillary vessels and the ratio of vessels to cardiomyocytes in the border area at 7 days after MI (Figure 4A). Moreover, EPO significantly increased the number of α-SMA–positive vessels in the heart 14 days after MI (Figure 4B), suggesting that EPO induces the formation of mature vessels in infarcted hearts.

We also investigated the effects of EPO-induced angiogenesis on myocardial perfusion. At 14 days after MI, the coronary flow under dilatory stimulation with sodium nitroprusside was significantly increased in EPO-treated hearts compared with saline-treated hearts in the isolated heart perfusion system (Figure 4C). The extent of myocardial ischemia in the border area detected by Hypoxyprobe staining was decreased by EPO treatment (Figure 4D), suggesting that EPO-induced angiogenesis is functionally relevant to the enhancement of coronary perfusion reserve and the reduction of cardiac ischemia in infarcted hearts. Meanwhile, there were no significant differences in the cross-sectional area of cardiomyocytes in the border area at 14 days after MI between EPO and saline treatment (Supplemental Figure 3).

We also examined the mechanisms of EPO-induced angiogenesis in vitro using HUVECs. The administration of EPO did not increase BrdU incorporation into HUVECs. In contrast, the culture medium of cardiomyocytes conditioned by EPO markedly enhanced the BrdU incorporation into HUVECs compared with the cultured medium of cardiomyocytes conditioned by saline (Figure 5A). The conditioned medium from EPO-treated cardiomyocytes also significantly enhanced tube formation of HUVECs, whereas the administration of EPO itself did not affect tube formation of HUVECs cultured in the medium from saline-treated cardiomyocytes (Figure 5B). These results suggest that EPO evokes an angiogenic response by inducing paracrine factors secreted from cardiomyocytes.

EPO upregulated the levels of VEGF in cultured cardiomyocytes in both time- and dose-dependent manners (Figure 5C). EPO also upregulated the levels of angiopoietin-1 (*Ang-1*) mRNA in cardiomyocytes, as evidenced by quantitative RT-PCR (qRT-PCR) (Figure 5D). Proliferation and tube formation of HUVEC induced by the conditioned medium from EPO-treated cardiomyocytes were significantly suppressed by a VEGF-specific inhibitor (CBO-P11) or an anti-Ang-1 antibody (Figure 5, A and B). Additionally, when VEGF was knocked down in cardiomyocytes using siRNA, the EPO-induced proliferation of HUVECs was also suppressed (Supplemental Figure 4A). These results suggest that VEGF and Ang-1 secreted from cardiomyocytes mediate the EPO-induced angiogenic response.

Consistent with the in vitro results, EPO treatment markedly increased the levels of VEGF and Ang-1 proteins and *Ang-1* mRNA in the heart after MI (Figure 5, E–G). To determine the role of EPO-mediated VEGF expression in vivo, we injected an adenoviral vector encoding a soluble form of Flt-1, an inhibitor of VEGF, into the thigh muscles of WT mice 4 days before and 3 days after MI. The beneficial effects of EPO on infarcted hearts, including increased vessel number, reduced infarct size, and improved cardiac function, were all abolished by VEGF inhibition (Figure 6), suggesting that VEGF secreted from cardiomyocytes plays a critical role in the cardioprotective effects of EPO against MI.

Shh is a critical mediator of the angiogenic effects of EPO. We further investigated how EPO increases angiogenic cytokine levels in infarcted hearts. Since Akt and ERK, which are activated by EPO, have been reported to regulate VEGF expression (19, 20), we first determined whether EPO increased expression levels of VEGF by activating these kinases in cardiomyocytes. Although both Akt and ERK were activated by EPO in cultured cardiomyocytes, activation levels were not so high as compared with other growth factors such as insulin (Supplemental Figure 2B and data not shown). Since EPO-induced upregulation of VEGF was so robust, we hypothesized that other mitogens mediate the EPO-induced upregulation of VEGF. It has recently been reported that carbamylated EPO (CEPO) promotes neural progenitor cell proliferation and their differentiation into neurons through an upregulation of Shh expression (21). Shh, a critical regulator of patterning and growth in various tissues during embryogenesis, has been reported to show angiogenic effects in infarcted hearts (22, 23). We thus examined the involvement of Shh signaling in EPO-induced cardioprotection.

To determine whether EPO upregulates Shh expression in cardiomyocytes, we first examined the levels of Shh in cultured cardiomyocytes. Both EPO and CEPO induced a marked accumulation of the biologically active, aminoterminal fragment of Shh

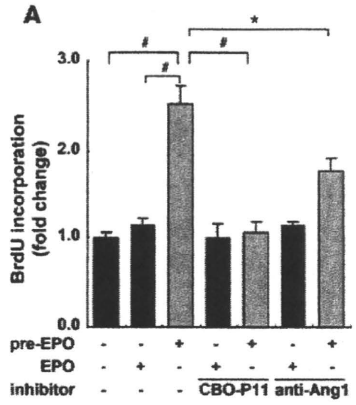

Figure 5

EPO upregulates angiogenic cytokine levels in cardiomyocytes and infarcted heart. (**A**) Endothelial cell proliferation assay using BrdU incorporation. Cardiomyocytes were pretreated with EPO (10 U/ml) or saline for 48 hours. HUVECs were treated with EPO-pretreated conditioned medium (pre-EPO) or saline-pretreated medium with EPO (EPO). Specific inhibitors of VEGF (CBO-P11) and Ang-1 (anti–Ang-1 antibody) were added to the culture medium as indicated. Data from a representative experiment are shown ($n = 5$ per condition). $^*P < 0.05$; $^\#P < 0.01$. (**B**) Tube formation assay. Quantification of tube length in HUVECs cultured with the conditioned medium was described in **A**. Data from a representative experiment are shown ($n = 3$ per condition). (**C**) Western blotting and quantification of VEGF levels from cultured cardiomyocytes treated with EPO. Time (at dose of 100 U/ml EPO) and dose (treated for 48 hours) dependency are shown ($n = 3$). $^*P < 0.05$ versus control. (**D**) qRT-PCR analysis of *Ang-1* mRNA from cultured cardiomyocytes treated with EPO ($n = 4$). Shown are levels of VEGF protein (**E**), Ang-1 mRNA (**F**), and protein (**G**) in the heart after MI. Representative Western blots and quantification are shown. WT mice were subjected to MI and treated with EPO or saline (control) ($n = 4$–5 for each condition).

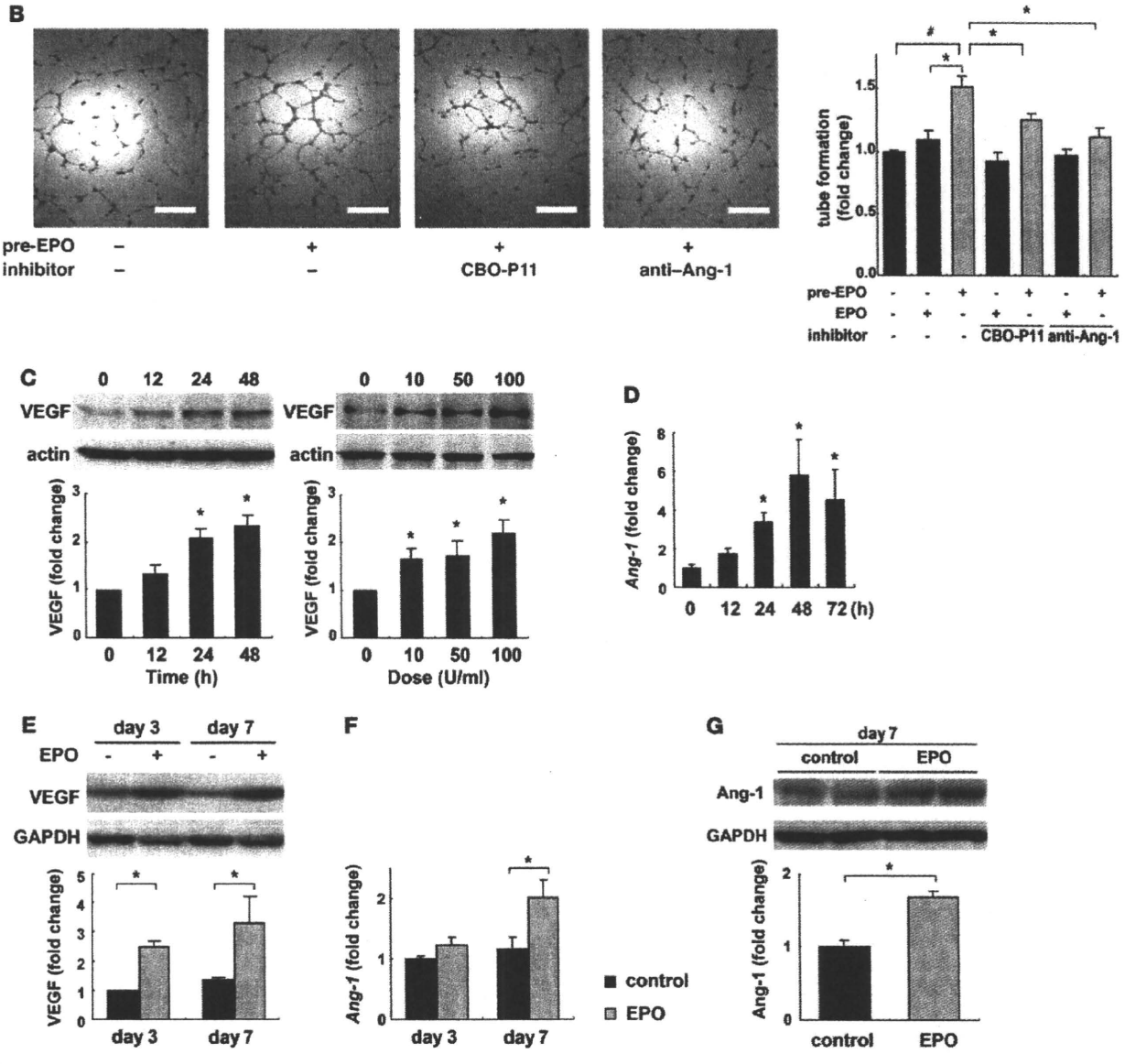

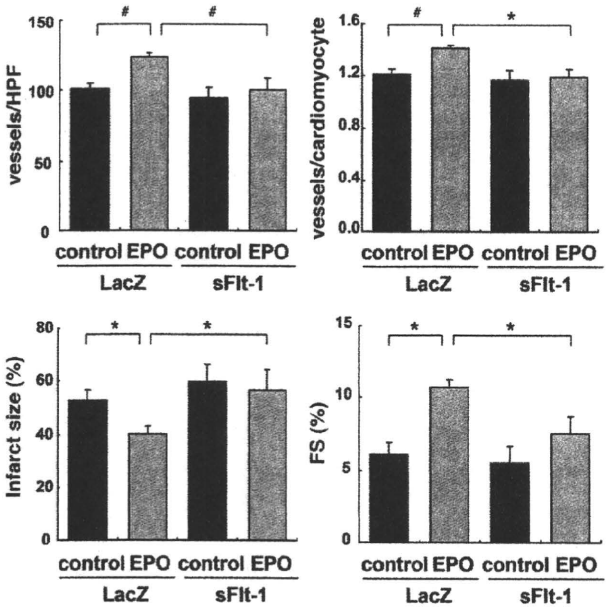

Figure 6

VEGF is essential for the angiogenic and cardioprotective effects of EPO. WT mice were injected with adenoviral vectors encoding soluble Flt-1 (sFlt-1) or LacZ, subjected to MI, and treated with EPO or saline (control). Echocardiographic analysis and immunohistochemical staining were then performed ($n = 8$). $^*P < 0.05$; $^\#P < 0.01$.

(Shh-N) in cardiomyocytes but not in cardiac fibroblasts 48 hours after treatment (Figure 7A), and Shh-N was abundantly secreted from EPO-treated cardiomyocytes into the culture medium (Figure 7B). Immunocytochemical analysis demonstrated that EPO induced the accumulation of Shh in α-sarcomeric actinin–positive cardiomyocytes but not in vimentin-positive cardiac fibroblasts (Figure 7C). In addition, EPO treatment significantly upregulated the levels of *Shh* mRNA in cardiomyocytes (Figure 7D).

We next determined whether Shh augmented angiogenic cytokine levels in cultured cardiomyocytes. Addition of recombinant murine Shh-N peptide (rmShh) increased the mRNA levels of the downstream target genes *Ptch1* and *Gli1* in cardiomyocytes in a dose-dependent manner (Figure 7E). rmShh also increased the levels of VEGF protein and *Ang-1* mRNA in cardiomyocytes as well as the concentration of VEGF protein in the culture medium (Figure 7, E and F). These changes were blocked by cyclopamine, a specific inhibitor of Shh signaling (Figure 7, E and F).

Cyclopamine treatment also significantly inhibited the EPO-induced increases in the levels of VEGF protein and *Ang-1* mRNA (Figure 8, A and B). Moreover, cyclopamine significantly inhibited the proliferation of HUVEC induced by conditioned medium from cardiomyocytes pretreated with EPO (Figure 8C). Consistently, knockdown of Shh in cardiomyocytes also inhibited the EPO-induced proliferation of HUVEC (Supplemental Figure 4B), indicating that EPO induces expression of angiogenic cytokines by activating Shh signaling in cardiomyocytes.

On the other hand, the EPO-induced inhibition of cardiomyocyte apoptosis 24 hours after exposure to H_2O_2 was not affected by cyclopamine (Figure 8D), suggesting that EPO shows its antiapoptotic effects on cardiomyocytes through a Shh-independent pathway.

Cardiomyocyte-specific Shh deletion abolishes EPO-induced cardioprotection. We next determined the role of Shh signaling in EPO-induced cardioprotection in vivo. The expression levels of Shh and Patched were increased in infarcted hearts (Figure 9A), as previously reported (23). Notably, expression levels of Shh and Patched protein were higher in infarcted hearts treated with EPO than in those treated with saline (Figure 9A), indicating that EPO activates Shh signaling in infarcted hearts. Meanwhile, there were no differences in the expression levels of Shh protein in the infarcted hearts of WT and RES mice, suggesting that endogenous EPO signaling is not associated with the upregulation of Shh in the infarcted hearts (Supplemental Figure 5).

Systemic deletion of Shh has been reported to result in cardiovascular defects in mice (24). To elucidate the roles of EPO-induced activation of Shh signaling pathways in infarcted hearts, we employed Shh-MerCre mice in which Shh is deleted only in cardiomyocytes following tamoxifen treatment. We crossed $Shh^{floxed/floxed}$ mice (25) with the transgenic mice in which a transgene encoding Cre recombinase was fused to the mutated estrogen receptor domains (MerCreMer) driven by the cardiomyocyte specific α-myosin heavy chain (α-MHC) promoter (26), and then produced the MHC-MerCreMer; $Shh^{floxed/floxed}$ mutant (Shh-MerCre) mice. After tamoxifen treatment, we confirmed that EPO-induced increases in the expression levels of Shh protein were significantly attenuated in the infarcted hearts of Shh-MerCre mice (Figure 9B). Under basal conditions at 7 days after tamoxifen treatment and at 14 days after MI, there were no significant differences in LV function or the number of vessels and the ratio of vessels to cardiomyocytes among Shh-MerCre mice, $Shh^{floxed/floxed}$ mice, MHC-MerCreMer mice, and WT mice (Figure 9, C and D, and data not shown).

There were no significant differences in LVEDD, FS, and infarct size in the Shh-MerCre mice treated with or without EPO after MI (Figure 9C). EPO did not increase the number of vessels, the ratio of vessels to cardiomyocytes, and the number of α-SMA–positive vessels in Shh-MerCre mice (Figure 9D). EPO treatment also failed to upregulate VEGF protein and *Ang-1* mRNA levels in Shh-MerCre mice (Figure 9, E and F), suggesting that myocardial Shh signaling is critical for the angiogenic and cardioprotective effects of EPO in infarcted hearts.

The role of STAT3 in the mechanism of EPO-induced cardioprotection. We have recently reported that G-CSF prevents LV remodeling after MI through the JAK2/STAT3 pathway in cardiomyocytes (5). To determine whether STAT3 is also involved in cardioprotective effects of EPO, we produced an MI model in transgenic mice that express dominant negative STAT3 in cardiomyocytes under the control of the α-MHC promoter (dnSTAT3-Tg). In dnSTAT3-Tg mice, the EPO treatment reduced infarct size and ameliorated LV dysfunction and remodeling at 14 days after MI by the same degree as WT mice (Supplemental Figure 6A). Overexpression of dnSTAT3 had no effects on EPO-induced prevention of H_2O_2-induced apoptotic death in cardiomyocytes (Supplemental Figure 6B), indicating that STAT3 is not involved in the mechanism of EPO-induced cardioprotective effects after MI.

Discussion

In the present study, we elucidated what we believe are novel mechanisms underlying the EPO-mediated inhibition of cardiac remodeling after MI. EPO enhanced the expression of angiogenic cytokines such as VEGF and Ang-1 in cultured cardiomyocytes and infarcted hearts, which, in turn, induced the proliferation of vas-

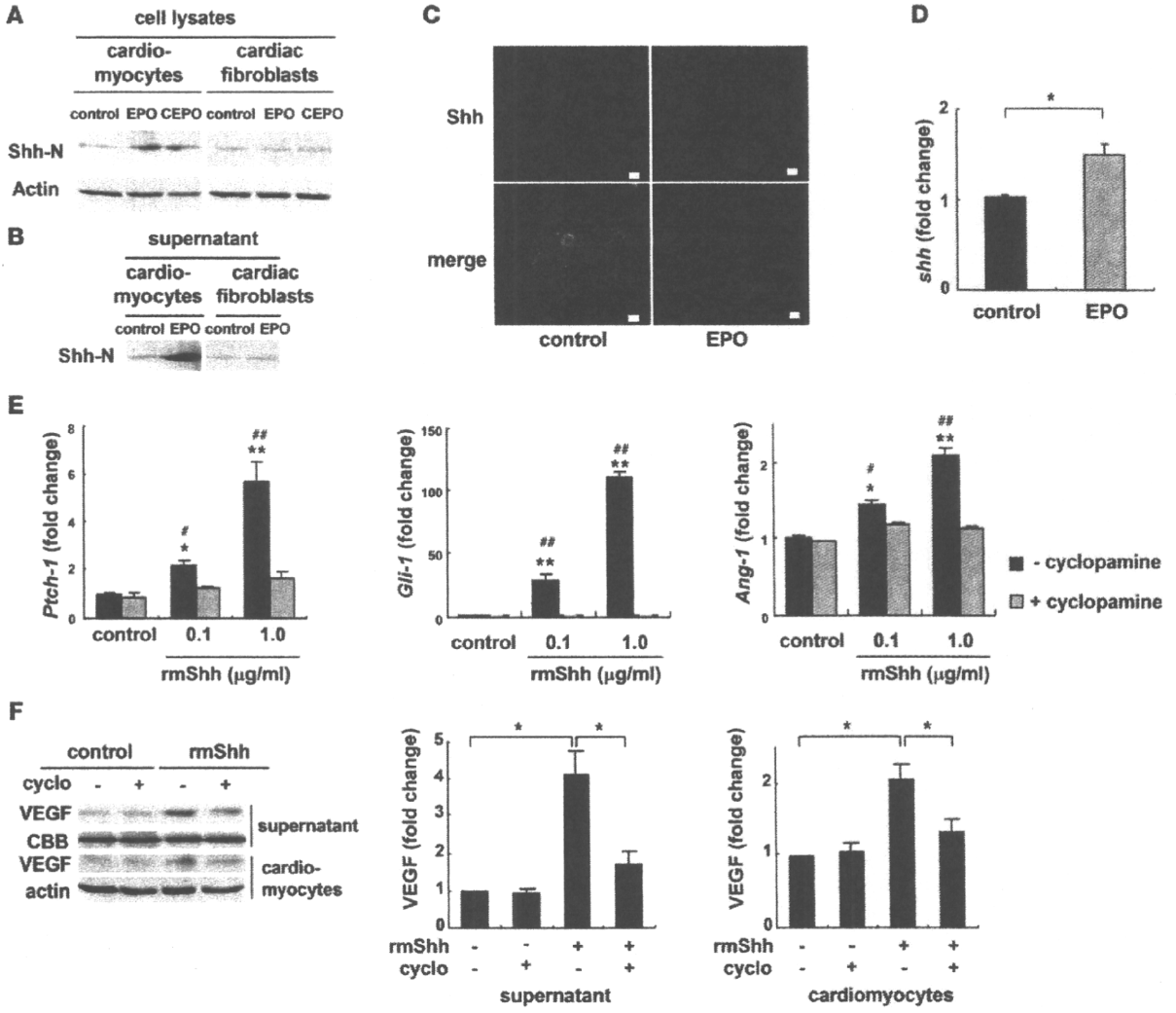

Figure 7

EPO upregulates expression levels of Shh. Western blotting of Shh in cultured neonatal rat cardiomyocytes and cardiac fibroblasts (**A**) and in the culture supernatants (**B**). Cells were treated with EPO (100 U/ml) or CEPO (100 U/ml) for 48 hours. Shh-N represents the aminoterminal domain of Shh, which is a biologically active form of Shh. (**C**) Immunocytochemical staining for Shh (red), α-sarcomeric actinin (green), and vimentin (blue). Cardiomyocytes and cardiac fibroblasts were cocultured with or without EPO for 48 hours. EPO induced the cytoplasmic accumulation of Shh in cardiomyocytes but not cardiac fibroblasts. Scale bars: 10 μm. (**D**) qRT-PCR analysis of *Shh* mRNA. Cardiomyocytes were treated with EPO for 24 hours ($n = 5$). $^*P < 0.05$. (**E**) qRT-PCR analysis of *Ptch-1*, *Gli-1*, and *Ang-1* mRNA. Cardiomyocytes were treated with rmShh (0.1 or 1.0 μg/ml) for 24 hours ($n = 4$). $^*P < 0.05$; $^{**}P < 0.01$ versus control. $^{\#}P < 0.05$; $^{\#\#}P < 0.01$ versus rmShh and cyclopamine (5 μM) treatment. (**F**) Western blotting of VEGF. Cardiomyocytes were treated with rmShh (1.0 μg/ml) for 48 hours. Cyclopamine (cyclo) was administered 15 minutes before rmShh treatment. Representative Western blots and quantification of the bands are shown ($n = 4$).

cular endothelial cells and angiogenesis. EPO also increased Shh levels in cardiomyocytes, and the various effects evoked by EPO were attenuated by inhibiting Shh signaling (Figure 9G).

We found that EPO promoted angiogenesis by upregulating the expression of VEGF and Ang-1. VEGF is a key molecule that initiates proliferation and migration of endothelial cells and promotes the formation of new vessels, whereas chronic VEGF overexpression in mice has been reported to produce numerous small vessels lacking functional layers (27). Ang-1 induces recruitment of smooth muscle cells to primitive vessels consisting of endothelial cells (27–29). Therefore, our results suggest that EPO treatment might be a better approach to creating stable and functional vessels in infarcted myocardium than the treatment with single angiogenic cytokine. Inhibition of angiogenesis by using the inhibitor of VEGF significantly attenuated the protective effects of EPO, such as the reduction of infarct size and improvement of LV function after MI. Since sufficient coronary perfusion resulting from angiogenesis can prevent cardiomyocyte apoptosis and improve contractile function (30, 31), angiogenic effects as well as direct antiapoptotic effects of EPO might protect the heart after MI. In this study, EPO did not enhance the homing of bone marrow–derived cells in damaged hearts, although EPO induced

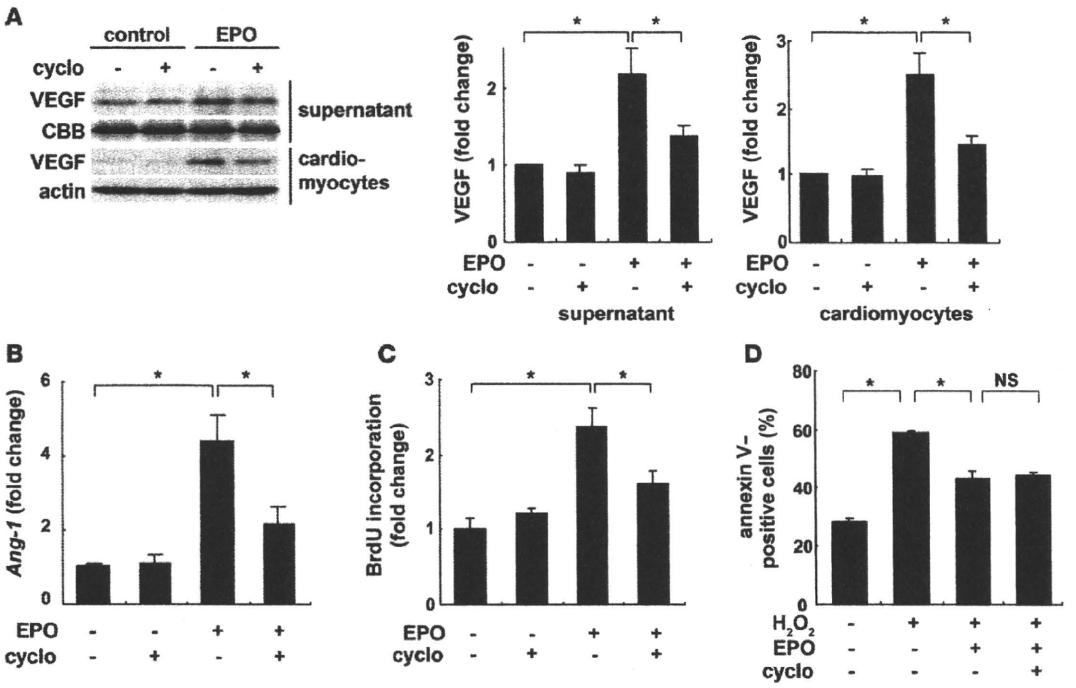

Figure 8

Shh is a critical mediator of the angiogenic effects of EPO in vitro. The expression levels of VEGF protein (**A**) and *Ang-1* mRNA (**B**). Cardiomyocytes were treated with EPO for 48 hours. Cyclopamine (5 μM) was added before EPO treatment. Quantification of the bands is shown ($n = 4$). *$P < 0.05$. (**C**) HUVEC proliferation assay. HUVECs were treated with cardiomyocyte-conditioned medium. Cyclopamine was added before EPO treatment. $n = 5$ per condition. (**D**) Detection of apoptosis using Cy3-labeled annexin V. Quantitative analysis is shown ($n = 6$).

mobilization of bone marrow cells including EPCs from bone marrow into peripheral circulation. It was previously reported that intramyocardial gene transfer of Shh enhanced angiogenesis by bone marrow–derived endothelial cells (23). Although reasons for the different results are not clear at present, the discrepancy may come from expression levels of Shh. Expression levels of Shh produced by intramyocardial gene transfer might be much higher than those induced by subcutaneous injection of EPO, and mode of actions of Shh (i.e., autocrine, paracrine, and endocrine) may be dependent on the expression levels of Shh.

EPO upregulated expression of Shh in cardiomyocytes, which played a critical role in protection of the heart after MI by increasing angiogenic cytokine production. In infarcted hearts, expression levels of Shh and its downstream target Patched have been reported to be increased (23), and Shh has been shown to produce robust angiogenic effects (22, 23). A recent study has demonstrated that cardiomyocyte-specific deletion of *Smoothened*, an essential component of Shh signaling, reduces the expression of angiogenic genes and the number of coronary vessels, resulting in cardiomyocyte apoptosis and cardiac dysfunction, and that vascular smooth muscle cell–specific deletion of *Smoothened* does not affect angiogenesis and cardiac function (32). These results and observations suggest that Shh upregulated by EPO in cardiomyocytes acts on cardiomyocytes themselves in an autocrine manner and increases production of angiogenic cytokines. There were no significant differences in size and function of LV and infarct size among the Shh-MerCre mice, $Shh^{floxed/floxed}$ mice, and MHC-MerCreMer mice without EPO after MI. It has been demonstrated that hedgehog, which is produced mainly by fibroblasts, is critical for maintenance and survival of the coronary vasculature in the adult heart and that the inhibition of endogenous hedgehog by anti-Shh antibody deteriorated cardiac function and induced enlargement of infarct area in the post-MI hearts (32). The discrepancy may come from the different cells of Shh inhibition. Secretion of Shh from other cells including fibroblasts was not inhibited in the cardiomyocyte-specific Shh-deleted mice (Shh-MerCre mice). In neural stem cells, Shh expression is induced via the Notch receptor–mediated activation of cytoplasmic signaling molecules, including Akt, STAT3, and mammalian target of rapamycin (33). Furthermore, it has been also reported that *Shh* is a target gene of NF-κB in mice (34). EPO is known to activate several signaling pathways, including Akt, STAT, and NF-κB in various tissues (19, 35). Further studies are needed to clarify the signaling cascade by which EPO upregulates Shh expression in cardiomyocytes.

We previously demonstrated that angiogenesis promotes cardiac hypertrophy in mice during the early phase of pressure overload (30). We do not know why EPO did not induce cardiomyocyte hypertrophy in this study, but there is a possibility that MI itself induces cardiac and cardiomyocyte hypertrophy via increased wall stress, and EPO-induced reduction of infarct size might reduce the wall stress, resulting in prevention of cardiac and cardiomyocyte hypertrophy even with enhanced angiogenesis.

In conclusion, EPO prevented LV remodeling after MI through Shh. We have reported that G-CSF inhibits cardiomyocyte apoptosis by activating the JAK2/STAT3 pathway in cardio-

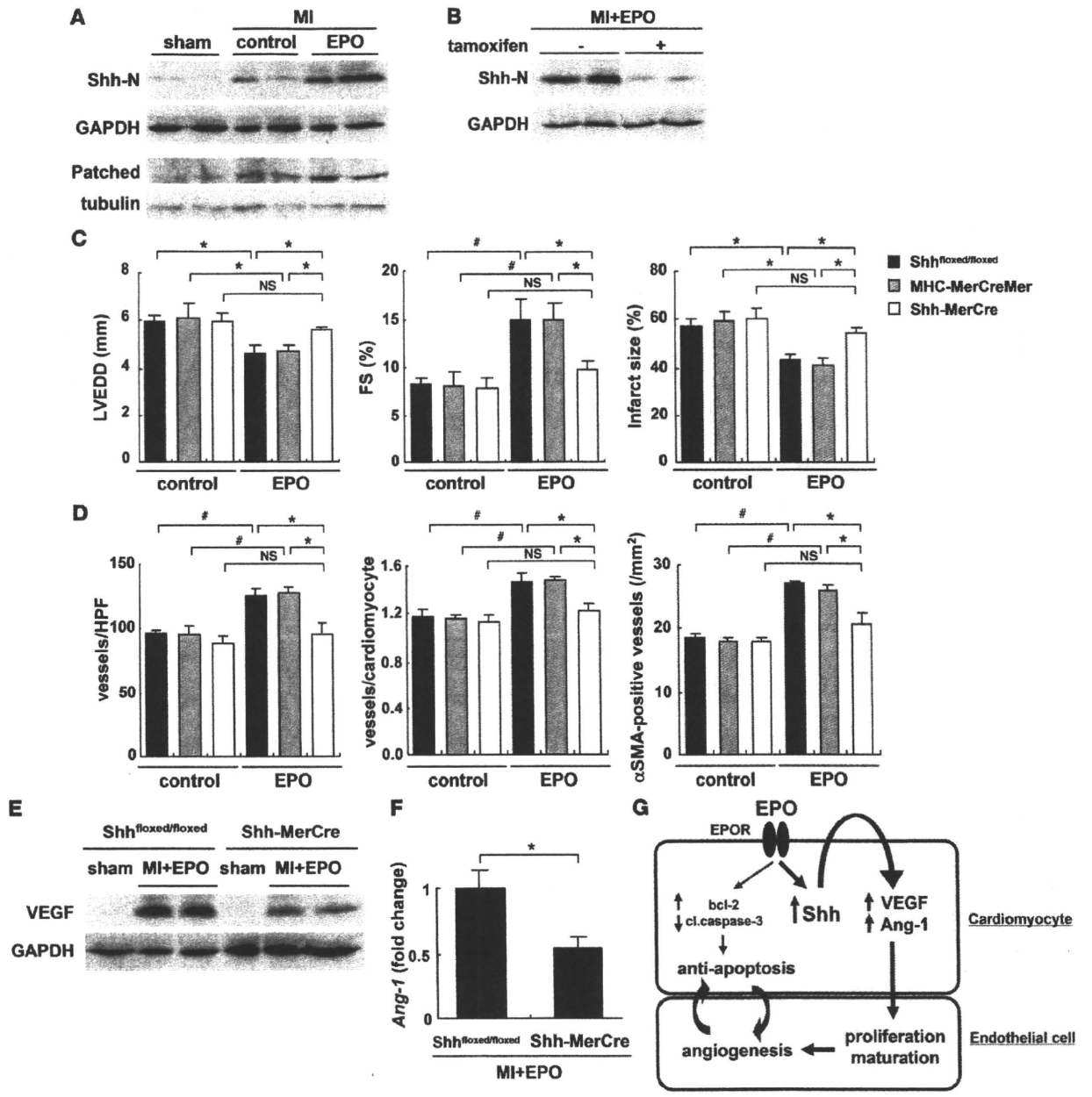

Figure 9

Cardiomyocyte-specific Shh deletion abolishes EPO-induced cardioprotection. (**A**) Activation of Shh signaling after MI and EPO treatment. Hearts were treated with EPO or saline (control) and harvested 4 days (for Shh-N) or 7 days (for Patched) after MI ($n = 4$ for each). (**B**) Western blotting of Shh-N in the infarcted hearts from Shh-MerCre mice treated with or without tamoxifen. Mice were subjected to MI, treated with EPO, and sacrificed 4 days after MI ($n = 4$ for each condition). We measured LVEDD, FS, infarct size (**C**), the number of vessels, the ratio of vessels to cardiomyocyte, and the number of α-SMA–positive vessels (**D**) 14 days after MI ($n = 8$–14). $^*P < 0.05$; $^\#P < 0.01$. (**E** and **F**) Western blotting of VEGF and qRT-PCR analysis of *Ang-1* mRNA in the heart 7 days after MI. All mice were treated with EPO ($n = 5$). $^*P < 0.05$. (**G**) Proposed mechanism underlying the cardioprotective effects of EPO during MI. The mechanisms denoted by the thicker lines are thought to be particularly important.

myocytes, leading to reduced LV remodeling (5). EPO prevented cardiomyocyte apoptosis and protected the heart via the JAK2/STAT3-independent mechanisms, presenting the possibility that administration of the 2 cytokines synergistically protects the heart after MI.

Methods

Animals. All experimental procedures were performed according to the guidelines established by Chiba University for experiments in animals, and all protocols were approved by our institutional review board. Male (C57BL/6 background, 10- to 12-week-old) mice were used in this study.

Shh$^{floxed/floxed}$ mice were purchased from Jackson Laboratory. We injected each mouse with 8 mg/kg of tamoxifen (Sigma-Aldrich) for 12 consecutive days and produced MI at 7 days after tamoxifen treatment. Because EPOR-null mice are embryonic lethal due to severe anemia, we prepared RES mice expressing EPOR exclusively in the hematopoietic lineage, which were established as described previously (15). EPOR expression is limited to the erythroid lineage cells in the RES mice. The RES mice develop normally and are fertile. GFP transgenic mice were purchased from SLC. Generation and genotyping of dnSTAT3-Tg mice have been previously described (36). Age- and sex-matched WT mice (C57BL/6; SLC) were used as controls. RES mice were provided by M. Yamamoto (Tohoku University School of Medicine, Miyagi, Japan).

Induction of MI and treatment. Mice were anesthetized by intraperitoneal injection of pentobarbital (50 mg/kg) and artificially ventilated with a respirator. Mice were subjected to ligation of the left anterior descending artery or to sham operation as described previously (4). Sham operation was performed by cutting pericardium. EPO (Chugai Pharmaceutical) or the same volume of saline was administered subcutaneously.

Echocardiography. Transthoracic echocardiography was performed with a VisualSonics (Vevo 660; VisualSonics Inc.) equipped with a 25-MHz imaging transducer. Mice were kept awake without anesthesia during the echocardiographic examination to minimize data deviation, and heart rate was approximately 550–650 bpm in all mice.

Histology. Hearts fixed in 10% formalin were embedded in paraffin and sectioned at 4-μm thickness for Masson trichrome staining. Tissue hypoxia was evaluated using the Hypoxyprobe (Chemicon) according to the manufacture's instructions. Fixed frozen sections of the heart samples were immunohistochemically stained by using primary antibodies to PECAM (Pharmingen), dystrophin (Novocastra Laboratories), α-SMA (DAKO), and Mac3 (BD Biosciences). The ischemic area that indicates infarct and border area was measured. For measurement of the cross-sectional area of cardiomyocytes, 50 randomly selected cardiomyocytes in a LV cross-section were measured by tracing dystrophin immunostaining. These measurements were performed with NIH ImageJ software. The samples were stained with Hoechst 33258 (1 μg/ml) or TO-PRO-3 (Molecular Probes Inc.). Immunofluorescence was visualized by laser confocal microscopy (Radiance 2000; Bio-Rad Laboratories).

Bone marrow transplantation. Bone marrow cells were isolated from 8-week-old transgenic mice systemically expressing GFP or WT mice. Bone marrow cells (5×10^7 cells) suspended in 100 μl of PBS containing 3% FBS were injected intravenously into irradiated WT mice or RES mice. A flow cytometric analysis revealed that more 97% of bone marrow cells were derived from donor cells at 6 weeks after bone marrow transplantation.

Flow cytometry. Circulating EPCs derived from bone marrow were detected by flow cytometry using CD34/Flk-1 double labeling. Mice subjected to MI or sham operation were treated with EPO or saline for 3 days subsequent to the operation. Then the mice were sacrificed to collect peripheral blood. The nucleated cells were incubated with FITC-conjugated anti-CD34 monoclonal antibody and PE-conjugated anti-Flk-1 antibody (VEGFR2/KDR; BD Biosciences) for 60 minutes on ice and washed with PBS supplemented with 3% FBS. The labeled nucleated cells were analyzed by the EPICS ALTRA flow cytometer using EXPO32 software (Beckman Coulter).

Western blot analysis. Western blot analysis was performed as described previously (30). Briefly, the infarcted hearts were separated into 2 parts consisting of the ischemic and viable regions. Proteins extracted from the ischemic regions of the infarcted hearts of mice were subjected to SDS-PAGE and then transferred onto polyvinylidene difluoride membranes (GE Healthcare). The membranes were probed using a primary antibody against, Shh-N (5E1; Developmental Studies Hybridoma Bank), VEGF, Patched, GAPDH (Santa Cruz Biotechnology Inc.), Ang-1 (Rockland). and α-tubulin (Sigma-Aldrich). For in vitro study, primary antibodies against Shh, Akt, Bcl-2 (Santa Cruz Biotechnology Inc.), VEGF for rat (R&D systems), phospho-Akt, phospho-ERK, cleaved caspase-3 (Cell Signaling), ERK (Invitrogen), and actin (Sigma-Aldrich) were used. The ECL-plus system (GE healthcare) was used for detection. Coomassie Brilliant Blue (Wako Pure Chemical Industries) was used for staining total protein blot with culture medium supernatant of cardiomyocytes.

In vivo gene transfer. Soluble Flt-1 is known to bind to VEGF, thereby acting on as an inhibitor for VEGF (37). We injected an adenoviral vector encoding the murine soluble *Flt-1* gene (10^9 pfu; Invitrogen) into thigh muscles of mice at 4 days before MI and 3 days after MI. Adenoviral vector encoding LacZ (10^9 PFU) was used as control.

Cell culture. Cardiomyocytes prepared from ventricles of 1-day-old Wistar rats were plated onto 35-mm plastic culture dishes at a concentration of 1×10^5 cells/cm^2 and cultured in DMEM supplemented with 10% FBS at 37°C in a mixture of 95% air and 5% CO_2. The culture medium was changed to serum-free DMEM 24 hours before stimulation. rmShh peptide was purchased from R&D Systems. The plasmid of a truncated form of human EPOR was from Y. Nakamura (RIKEN BioResource Center, Tsukuba, Ibaraki, Japan) (38). Adenoviral vector of truncated EPOR was created using AdEasy Vector System (Qbiogene). Adenoviral vector of dnSTAT3 was a gift from K. Yamauchi-Takihara (Osaka University, Osaka, Japan) (36). siRNA targeting VEGF, Shh, and negative control RNA (Invitrogen) were introduced into rat cardiomyocytes by using Lipofectamine RNAiMAX (Invitrogen) according to the manufacturer's instructions. For immunocytochemical staining, cardiomyocytes and cardiac fibroblasts were cocultured with or without EPO for 48 hours, fixed in 4% paraformaldehyde, and stained with primary antibodies to Shh (Santa Cruz Biotechnology Inc.), α-sarcomeric actinin (Sigma-Aldrich), and vimentin (Progen).

qRT-PCR. qRT-PCR analysis was performed as described previously (39). Total RNA was extracted from sample using the RNeasy kit (QIAGEN). We used 2.5 μg of total RNA to generate cDNA using the Super Script VILO cDNA synthesis kit (Invitrogen). qRT-PCR was carried out on a LightCycler system (Roche) using probes from Universal Probe Library (Roche) and the TaqMan Master Mix (Roche). Sequence of primers and the respective Universal Probe Library probes were as follows: *Ang-1*: forward GGAAGATGGAAGCCTGGAT, reverse ACCAGAGGGATTCCCAAAAC, probe #12; *Gapdh*: forward TGTCCGTCGTGGATCTGAC, reverse CCTGCTTCACCACCTTCTTG, probe #80, each for mouse; *Shh*: forward GAATCCAAAGCTCGCATCC, reverse CAGGTGCACTGTGGCTGAT, probe #38; *Ang-1*: forward GGAAGCCTAGATTTCCAGAGG, reverse ACCAGAGGGATTCCCAAAAC, probe #12; *Ptch-1*: forward CAAAGCTGACTACATGCCAGA, reverse GCGTACTCTATGGGCTCTGC, probe #64, *Gli-1*: forward GGAAGAGAGCAGACTGACTGTG, reverse GGGGAGTGGTCACTGCTG, probe #1; and *Gapdh*: forward AATGTATCCGTTGTGGATCTGA, reverse GCTTCACCACCTTCTTGATGT, probe #80, each for rat. Relative expression of target genes was calculated with the comparative CT method. Each sample was run in duplicate, and the results were systematically normalized using *Gapdh*.

Apoptosis analysis. Frozen sections of the heart samples and cultured cardiomyocytes fixed by 4% paraformaldehyde were subjected to TUNEL staining using a commercially available kit (In Situ Apoptosis Detection Kit; Takara Biomedicals) as directed by manufacturer. Annexin V-Cy3 Apoptosis Detection Kit (BioVision) was used to detect apoptotic cardiomyocytes according to the manufacture's instructions. Cultured cardiomyocytes were serum starved in DMEM with 0.5% FBS and treated with EPO (10 U/ml) or normal saline for 8 hours prior to beginning H_2O_2 (100 μM) treatment. Cyclopamine (40–42) (5 μM), LY294002 (5 μM), and PD98059 (10 μM; Calbiochem) were administered 15 minutes before EPO treatment.

DNA synthesis assay. DNA synthesis was measured by performing a BrdU incorporation assay with a commercially available kit (Roche) as directed by the manufacturer. Cardiomyocyte-conditioned medium was collected as previously described (43). Briefly, cultured cardiomyocytes were starved in DMEM without FBS and were pretreated with EPO (10 U/ml) or saline for 48 hours, and then the medium was collected and transferred to HUVECs. HUVECs were plated in 96-well plates at a density of 5×10^4 cells/well in endothelial cell basal medium-2 with EGM-2 Bullet Kit (Cambrex) for 8 hours and then switched to cardiomyocyte-conditioned medium for 12 hours. BrdU was added to the medium, and BrdU incorporation was detected by ELISA using anti-BrdU antibody. VEGF receptor antagonist CBO-P11 (44, 45) (12 μM; Calbiochem) and anti-Ang-1 antibody (1 μg/ml; Chemicon) were used for the inhibition studies.

Tube formation assay. Matrigel (growth factor reduced, 100 μl; BD Biosciences) was added to each well of a 48-well plate and allowed to polymerize at 37°C for 1 hour. HUVECs (1×10^4) were seeded onto Matrigel in endothelial cell basal medium-2 with EGM-2 Bullet Kit and cultured for 1 hour and then switched to cardiomyocyte-conditioned medium described above. After 8 hours, tube length was quantified using an angiogenesis image analyzer (Kurabo).

Isolated heart perfusion system. Isolated heart perfusion system was used to measure coronary flow as previously described (46). In brief, mouse hearts were excised rapidly and mounted on a Langendorff perfusion system. All isolated hearts were stabilized by perfusion of Krebs-Henseleit buffer, and perfusion pressure was adjusted to 60 mmHg. The heart was paced at 400 bpm. After an adjustment period, the coronary effluent was collected and the coronary flow was calculated. After baseline measurements, sodium nitroprusside (10^{-4} M, Sigma-Aldrich) was infused into the perfusate, and coronary flow was measured.

Statistics. All data are shown as mean ± SEM. Multiple group comparison was performed by 1-way ANOVA followed by Bonferroni's procedure for comparison of means. Comparison between 2 groups was analyzed by the 2-tailed Student's *t* test. Values of $P < 0.05$ were considered statistically significant.

Acknowledgments

The authors thank M. Yamamoto (Tohoku University School of Medicine, Miyagi, Japan) for generously providing RES mice. The authors thank Y. Ohtsuki, M. Ikeda, I. Sakamoto, A. Furuyama, M. Kikuchi, and H. Maruyama for their excellent technical assistance. This work was supported by a Grant-in-Aid for Scientific Research from the Ministry of Education, Science, Sports, and Culture, and Health and Labor Sciences research grants (to I. Komuro) and a Grant-in-Aid for Scientific Research from the Ministry of Education, Culture, Sports, Science and Technology of Japan and grants from the Terumo Life Science Foundation (to H. Takano).

Received for publication May 18, 2009, and accepted in revised form March 24, 2010.

Address correspondence to: Issei Komuro, Department of Cardiovascular Science and Medicine, Chiba University Graduate School of Medicine, 1-8-1 Inohana, Chuo-ku, Chiba 260-8670, Japan. Phone: 81.43.226.2097; Fax: 81.43.226.2557; E-mail: komuro-tky@umin.ac.jp.

1. Jessup M, Brozena S. Heart failure. *N Engl J Med.* 2003;348(20):2007–2018.
2. Rosamond W, et al. Heart disease and stroke statistics--2008 update: a report from the American Heart Association Statistics Committee and Stroke Statistics Subcommittee. *Circulation.* 2008;117(4):e25–146.
3. Moon C, et al. Erythropoietin reduces myocardial infarction and left ventricular functional decline after coronary artery ligation in rats. *Proc Natl Acad Sci U S A.* 2003;100(20):11612–11617.
4. Ohtsuka M, et al. Cytokine therapy prevents left ventricular remodeling and dysfunction after myocardial infarction through neovascularization. *FASEB J.* 2004;18(7):851–853.
5. Harada M, et al. G-CSF prevents cardiac remodeling after myocardial infarction by activating the Jak-Stat pathway in cardiomyocytes. *Nat Med.* 2005;11(3):305–311.
6. Silverberg DS, et al. The effect of correction of mild anemia in severe, resistant congestive heart failure using subcutaneous erythropoietin and intravenous iron: a randomized controlled study. *J Am Coll Cardiol.* 2001;37(7):1775–1780.
7. Ponikowski P, et al. Effect of darbepoetin alfa on exercise tolerance in anemic patients with symptomatic chronic heart failure: a randomized, double-blind, placebo-controlled trial. *J Am Coll Cardiol.* 2007;49(7):753–762.
8. Felker GM, Adams KF Jr, Gattis WA, O'Connor CM. Anemia as a risk factor and therapeutic target in heart failure. *J Am Coll Cardiol.* 2004;44(5):959–966.
9. Bahlmann FH, et al. Erythropoietin regulates endothelial progenitor cells. *Blood.* 2004; 103(3):921–926.
10. Parsa C, et al. A novel protective effect of erythropoietin in the infarcted heart. *J Clin Invest.* 2003; 112(7):999–1007.
11. Wright GL, Hanlon P, Amin K, Steenbergen C, Murphy E, Arcasoy MO. Erythropoietin receptor expression in adult rat cardiomyocytes is associated with an acute cardioprotective effect for recombinant erythropoietin during ischemia-reperfusion injury. *FASEB J.* 2004;18(9):1031–1033.
12. Brines M, Cerami A. Emerging biological roles for erythropoietin in the nervous system. *Nat Rev Neurosci.* 2005;6(6):484–494.
13. Tada H, et al. Endogenous erythropoietin system in non-hematopoietic lineage cells plays a protective role in myocardial ischemia/reperfusion. *Cardiovasc Res.* 2006;71(3):466–477.
14. Asaumi Y, et al. Protective role of endogenous erythropoietin system in nonhematopoietic cells against pressure overload-induced left ventricular dysfunction in mice. *Circulation.* 2007;115(15):2022–2032.
15. Suzuki N, et al. Erythroid-specific expression of the erythropoietin receptor rescued its null mutant mice from lethality. *Blood.* 2002;100(7):2279–2288.
16. Li Y, et al. Reduction of inflammatory cytokine expression and oxidative damage by erythropoietin in chronic heart failure. *Cardiovasc Res.* 2006;71(4):684–694.
17. Hirose S, et al. Erythropoietin attenuates the development of experimental autoimmune myocarditis. *Cardiovasc Drugs Ther.* 2007;21(1):17–27.
18. Abbate A, Biondi-Zoccai GG, Baldi A. Pathophysiologic role of myocardial apoptosis in post-infarction left ventricular remodeling. *J Cell Physiol.* 2002;193(2):145–153.
19. Latini R, Brines M, Fiordaliso F. Do non-hemopoietic effects of erythropoietin play a beneficial role in heart failure? *Heart Fail Rev.* 2008;13(4):415–423.
20. Pagès G, Pouysségur J. Transcriptional regulation of the Vascular Endothelial Growth Factor gene--a concert of activating factors. *Cardiovasc Res.* 2005;65(3):564–573.
21. Wang L, et al. The sonic hedgehog pathway mediates carbamylated erythropoietin–enhanced proliferation and differentiation of adult neural progenitor cells. *J Biol Chem.* 2007;282(42):32462–32470.
22. Pola R, et al. The morphogen sonic hedgehog is an indirect angiogenic agent upregulating two families of angiogenic growth factors. *Nat Med.* 2001;7(6):706–711.
23. Kusano KF, et al. Sonic hedgehog myocardial gene therapy: tissue repair through transient reconstitution of embryonic signaling. *Nat Med.* 2005;11(11):1197–1204.
24. Washington Smoak I, et al. Sonic hedgehog is required for cardiac outflow tract and neural crest cell development. *Dev Biol.* 2005;283(2):357–372.
25. Lewis PM, et al. Cholesterol modification of sonic hedgehog is required for long-range signaling activity and effective modulation of signaling by Ptc1. *Cell.* 2001;105(5):599–612.
26. Sohal DS, et al. Temporally regulated and tissue-specific gene manipulations in the adult and embryonic heart using a tamoxifen-inducible Cre protein. *Circ Res.* 2001;89(1):20–25.
27. Suri C, et al. Increased vascularization in mice overexpressing angiopoietin-1. *Science.* 1998; 282(5388):468–471.
28. Asahara T, et al. Tie2 receptor ligands, angiopoietin-1 and angiopoietin-2, modulate VEGF-induced postnatal neovascularization *Circ Res.* 1998;83(3):233–240.
29. Holash J, Wiegand SJ, Yancopoulos GD. New model of tumor angiogenesis: dynamic balance between vessel regression and growth mediated by angiopoietins and VEGF. *Oncogene.* 1999;18(38):5356–5362.
30. Sano M, et al. p53-induced inhibition of Hif-1 causes cardiac dysfunction during pressure overload. *Nature.* 2007;446(7134):444–448.
31. Giordano FJ, et al. A cardiac myocyte vascular endothelial growth factor paracrine pathway is required to maintain cardiac function. *Proc Natl Acad Sci U S A.* 2001;98(10):5780–5785.
32. Lavine KJ, Kovacs A, Ornitz DM. Hedgehog signaling is critical for maintenance of the adult coronary vasculature in mice. *J Clin Invest.* 2008;118(7):2404–2414.
33. Androutsellis-Theotokis A, et al. Notch signaling regulates stem cell numbers in vitro and in vivo. *Nature.* 2006;442(7104):823–826.
34. Kasperczyk H, Baumann B, Debatin KM, Fulda S. Characterization of sonic hedgehog as a novel

NF-kappaB target gene that promotes NF-kappaB-mediated apoptosis resistance and tumor growth in vivo. *FASEB J.* 2009;23(1):21–33.
35. Digicaylioglu M, Lipton SA. Erythropoietin-mediated neuroprotection involves cross-talk between Jak2 and NF-kappaB signalling cascades. *Nature.* 2001;412(6847):641–647.
36. Funamoto M, et al. Signal transducer and activator of transcription 3 is required for glycoprotein 130–mediated induction of vascular endothelial growth factor in cardiac myocytes. *J Biol Chem.* 2000;275(14):10561–10566.
37. Kendall RL, Thomas KA. Inhibition of vascular endothelial cell growth factor activity by an endogenously encoded soluble receptor. *Proc Natl Acad Sci U S A.* 1993;90(22):10705–10709.
38. Nakamura Y, Komatsu N, Nakauchi H. A truncated erythropoietin receptor that fails to prevent programmed cell death of erythroid cells. *Science.* 1992;257(5073):1138–1141.
39. Leucht C, Stigloher C, Wizenmann A, Klafke R, Folchert A, Bally-Cuif L. MicroRNA-9 directs late organizer activity of the midbrain-hindbrain boundary. *Nat Neurosci.* 2008;11(6):641–648.
40. Taipale J, et al. Effects of oncogenic mutations in Smoothened and Patched can be reversed by cyclopamine. *Nature.* 2000;406(6799):1005–1009.
41. Berman D, et al. Medulloblastoma growth inhibition by hedgehog pathway blockade. *Science.* 2002;297(5586):1559–1561.
42. Watkins DN, Berman DM, Burkholder SG, Wang B, Beachy PA, Baylin SB. Hedgehog signalling within airway epithelial progenitors and in small-cell lung cancer. *Nature.* 2003;422(6929):313–317.
43. Zhang Y, Pasparakis M, Kollias G, Simons M. Myocyte-dependent regulation of endothelial cell syndecan-4 expression. Role of TNF-alpha. *J Biol Chem.* 1999;274(8):4786–4790.
44. Zilberberg L, et al. Structure and inhibitory effects on angiogenesis and tumor development of a new vascular endothelial growth inhibitor. *J Biol Chem.* 2003;278(37):35564–35573.
45. Heineke J, et al. Cardiomyocyte GATA4 functions as a stress-responsive regulator of angiogenesis in the murine heart. *J Clin Invest.* 2007;117(11):3198–3210.
46. Bendall J, et al. C. Strain-dependent variation in vascular responses to nitric oxide in the isolated murine heart. *J Mol Cell Cardiol.* 2002;34(10):1325–1333.

MOLECULAR AND CELLULAR BIOLOGY, Mar. 2011, p. 1054–1065 Vol. 31, No. 5
0270-7306/11/$12.00 doi:10.1128/MCB.00732-10

Increased Akt-mTOR Signaling in Lung Epithelium Is Associated with Respiratory Distress Syndrome in Mice[▽]

Hiroyuki Ikeda,[1,2] Ichiro Shiojima,[1,3] Toru Oka,[1,3] Masashi Yoshida,[1] Koji Maemura,[4] Kenneth Walsh,[5] Takashi Igarashi,[2] and Issei Komuro[1,3]*

Department of Cardiovascular Science and Medicine, Chiba University Graduate School of Medicine, Chiba, Japan[1]; Department of Pediatrics, University of Tokyo Graduate School of Medicine, Tokyo, Japan[2]; Department of Cardiovascular Medicine, Osaka University Graduate School of Medicine, Suita, Japan[3]; Department of Cardiovascular Medicine, Nagasaki University Graduate School of Biomedical Sciences, Nagasaki, Japan[4]; and Molecular Cardiology, Whitaker Cardiovascular Institute, Boston University School of Medicine, Boston, Massachusetts[5]

Received 24 June 2010/Returned for modification 31 August 2010/Accepted 17 December 2010

Pregnancy in women with diabetes is associated with a higher risk of perinatal complications. In particular, infants of diabetic mothers frequently suffer from respiratory distress syndrome (RDS), which is a leading cause of death in preterm infants and is considered to be primarily due to hyperinsulinemia in infants in response to maternal hyperglycemia. To elucidate the mechanism of how insulin signaling induces RDS, bronchoalveolar epithelium-specific Akt1 transgenic (TG) mice were generated. Akt1 overexpression in fetal lung epithelium resulted in RDS in preterm infants born by Caesarean section at embryonic day 18.5 (E18.5). The expression levels of hypoxia-inducible factor 2α (HIF-2α) and its target vascular endothelial growth factor (VEGF) were downregulated in the lung of Akt1 TG mice. Inhibition of the Akt-mammalian target of rapamycin (mTOR) signaling axis by rapamycin restored the expression of VEGF and improved the lung pathology of Akt1 TG pups. Rapamycin also attenuated the RDS phenotype in wild-type mice delivered preterm at E17.5. In cultured lung epithelial cells, insulin reduced VEGF expression and transcriptional activity of HIF-2 on *VEGF* promoter in an mTOR-dependent manner. Thus, aberrant activation of the Akt-mTOR pathway in lung epithelium plays a causal role in the pathogenesis of infant RDS, presumably through downregulation of HIF-2-dependent VEGF expression in the lung.

Pregnancy in women with diabetes is associated with a higher risk of perinatal complications. The estimated prevalence rate of gestational diabetes is approximately 4% and is considered to represent 90% of all cases of diabetes diagnosed during pregnancy (2). Moreover, pregnant women with type 2 diabetes are increasing in number in line with the rapid increase in the prevalence of type 2 diabetes in all age groups (9). Infants of diabetic mothers frequently suffer from macrosomia, neonatal hypoglycemia, cardiomegaly, respiratory difficulties, and other congenital anomalies (3, 5, 14, 21), which are considered to be primarily due to hyperinsulinemia in infants in response to maternal hyperglycemia. Respiratory distress syndrome (RDS) is one of the most clinically significant perinatal complications, with high morbidity and mortality (19, 22). RDS is caused by attenuated production of pulmonary surfactant, a mixture of phospholipids and surfactant-associated proteins that covers the alveolar surface and prevents alveolar collapse by reducing the surface tension of the air-water interface (12). Because pulmonary surfactant is specifically produced by type II lung epithelial cells, attenuated production of pulmonary surfactant is considered to be due to impaired differentiation and/or maturation of type II lung epithelial cells (31). Reduced expression of surfactant-associated proteins was observed in fetuses of streptozotocin-induced diabetic rats or in insulin-treated human fetal lung explants (8, 10, 11), suggesting that hyperactivation of insulin signaling in the lung plays a causal role in the pathogenesis of RDS of infants having a diabetic mother.

Phosphatidylinositol 3-kinase (PI3K) is activated by insulin and is responsible for most of the metabolic actions of insulin. PI3K also controls cell growth, differentiation, survival, and protein synthesis (28). The involvement of the PI3K pathway in RDS was suggested by a previous report showing that bronchoalveolar-specific deletion of *Pten* in mice led to upregulation of the PI3K pathway in the lung and resulted in RDS associated with marked hyperplasia of alveolar epithelial cells, increased numbers of bronchoalveolar stem cells (BASCs), and impaired production of surfactant proteins (SPs) (33). It was also shown that genetic ablation of hypoxia-inducible factor 2α (HIF-2α) causes RDS due to downregulation of vascular endothelial growth factor (VEGF) expression in the lung and that intratracheal VEGF administration stimulates maturation of type II lung epithelial cells (4). However, the downstream effectors of PI3K that cause RDS and the mechanistic link between the PI3K pathway and HIF-2-dependent VEGF expression in the lung have been elusive.

Using bronchoalveolar epithelium-specific Akt1 transgenic (TG) mice, we show here that aberrant activation of the Akt-mammalian target of rapamycin (mTOR) pathway in lung epithelium plays a causal role in the pathogenesis of infant RDS. We also provide evidence suggesting that sustained Akt-mTOR activation induces RDS through downregulation of HIF-2-dependent VEGF expression in the lung.

MATERIALS AND METHODS

Animals and DOX administration. SP-C-rtTA TG mice expressing the reverse tetracycline transactivator (rtTA) protein under the control of the human surfactant protein-C promoter (pro-SP-C) on the FVB/N background were de-

* Corresponding author. Mailing address: Department of Cardiovascular Medicine, Osaka University Graduate School of Medicine, 2-2 Yamadaoka, Suita 565-0871, Japan. Phone: 81 6 6879 3631. Fax: 81 6 6879 3639. E-mail: komuro-tky@umin.ac.jp.

▽ Published ahead of print on 28 December 2010.

scribed previously (23, 29) and were purchased from the Jackson Laboratory. These mice were crossed with Tet-myrAkt1 TG mice (25) harboring a myristoylated Akt1 (myrAkt1) transgene under the control of multimerized *tetO* sequences maintained on a mixed background of FVB/N, C57BL/6J, and 129Sv. For myrAkt1 expression, dams were treated with doxycycline (DOX) in drinking water from embryonic day 0.5 (E0.5) at a final concentration of 0.5 mg/ml (25, 29). Respiratory rate was measured by visual inspection of the movements of thorax and abdomen for 1 min. All animal procedures were performed with the approval of the Institutional Animal Care and Use Committee of Chiba University.

Histological analysis and immunohistochemistry. Lungs were formalin fixed without constant pressure inflation and embedded in paraffin for histological analyses. Serial sections of 4 μm were stained with hematoxylin and eosin (HE) for morphological analysis, periodic acid-Schiff (PAS) for detection of glycogen-rich cells, and Masson's trichrome (MT) for detection of fibrosis. Aerated lung area and alveolar septal thickness were measured in toluidine blue-stained sections using ImageJ software (4). Aerated lung area was measured in 10 visual fields for each animal. Septal thickness was measured at 10 points in each visual field, and 10 visual fields for each animal were used for the measurement. The size and number of saccules were measured in PAS-stained sections using ImageJ software. The size of 10 saccules was measured in each visual field, and 10 visual fields for each animal were used for the analysis. Saccular number was counted in 10 visual fields for each animal. Immunohistochemistry was performed using an avidin-biotin-horseradish peroxidase detection system with Ni-diaminobenzidine (DAB) (ABC kit; Vector Laboratories) and Nuclear Fast Red as a counterstain. The antibodies used were hemagglutinin (HA), pro-SP-C, Clara cell 10-kDa protein (CC10), aquaporin-5 (AQP5), VEGF (Santa Cruz Biotechnology), and calcitonin gene-related peptide (CGRP; BioMol).

Fluorescence imaging. A BZ-9000 (Keyence) microscope was used for fluorescence imaging. Paraffin-embedded lung sections were incubated with isolectin B4-fluorescein isothiocyanate (FITC) conjugate (Sigma) to detect endothelial cells and with wheat germ agglutinin-tetramethyl rhodamine isothiocyanate (TRITC) conjugate (Sigma) to counterstain the cell membrane. Vascular cell counts with three replications were performed with BZ application software (Keyence), and the median value was used for each sample.

Western blot analysis. Total protein lysate was extracted from lung tissue, and SDS-PAGE was performed as described previously (26). The antibodies used were HA, total Akt1, total S6 kinase (S6K), SP-A, pro-SP-C, AQP5, CC10, VEGF, glyceraldehyde-3-phosphate dehydrogenase (GAPDH; Santa Cruz Biotechnology), phospho-Akt (Ser473), phospho-S6K1 (Thr389), phospho-S6 (Ser235/236), total S6, phospho-glycogen synthase kinase 3β (phospho-GSK3β) (Ser9), phospho-FOXO3a (318/321), total FOXO3a (Cell Signaling Technology), SP-B, SP-D (Chemicon/Millipore), and HIF-2α (Novus Biologicals). Densitometric analysis was performed using ImageJ.

Mouse model of preterm infants. Pups were collected by Caesarean section at E18.5 for Akt1 TG mice and at E17.5 for wild-type ICR mice (4, 20). The umbilical cord was cut, amniotic fluid and membranes were removed from the mouth and nose, and body temperature was kept at 37°C.

Administration of rapamycin. Rapamycin (LC Laboratories) was prepared in the solvent containing 0.2% sodium carboxymethylcellulose and 0.25% polysorbate-80 in water (24, 25). Rapamycin (1 mg/kg of body weight/day) or vehicle was administered subcutaneously to dams.

Reporter gene assays. Luciferase assays were performed essentially as previously described (18). The plasmids used were VEGF reporter plasmid (pGL2hVEGF) and the expression vectors for HIF-1α (phHIF-1α), HIF-2α (phEP-1), and ARNT (phARNT). A549 cells were transfected with the plasmids indicated in the Fig. 8 legend and treated with 250 μM $CoCl_2$ to mimic hypoxic condition.

Statistical analysis. Data are expressed as means ± standard errors of the means (SEM). Statistical significance between two groups was determined with a Student's *t* test or χ^2 test. Probability values of <0.05 were considered to be statistically significant.

RESULTS

Generation of bronchoalveolar epithelium-specific Akt1 TG mice. Two lines of TG mice (Tet-myrAkt1 and SP-C-rtTA) were used to generate bronchoalveolar epithelium-specific Akt1 TG mice (Fig. 1A). The Tet-myrAkt1 TG line harbors an active form of the Akt1 transgene (myrAkt1) under the control of multimerized tetracycline operator (*tetO*) sequences (25), and the SP-C-rtTA TG line expresses the reverse tetracycline transactivator (rtTA) in respiratory epithelial cells driven by human surfactant protein-C (SP-C) promoter (23, 29). DOX enables rtTA binding to *tetO* sequences by inducing its conformational change. Therefore, DOX treatment of double-TG (DTG) mice harboring both transgenes induces transcription of the myrAkt1 gene in lung epithelial cells (Fig. 1A). Mating of SP-C-rtTA mice with Tet-myrAkt1 mice resulted in the generation of mice with four different genotypes (wild type, Tet-myrAkt1 single TG, SP-C-rtTA single TG, and DTG) at the expected frequencies. Western blot analysis of lung lysates harvested at postnatal day 0 (P0) revealed that the transgene product detected by anti-HA blotting was observed in the lung of DTG mice treated with DOX (Fig. 1B). The induced expression of myrAkt1 was associated with a marked increase in phosphorylation levels of several downstream effectors such as S6K1, S6, and glycogen synthase kinase-3 (GSK3), but not FOXO3 (Fig. 1B). Because it was reported that treatment of SP-C-rtTA mice with DOX may exert toxic effects on alveolar epithelial cells (20), the phenotype of DOX-treated SP-C-rtTA single-TG mice was carefully compared with littermates of other genotypes (wild type, Tet-myrAkt1 single TG, and DTG). However, although there was an obvious lung phenotype in DTG mice (described in detail below), no apparent abnormality was observed in mice with other genotypes under our experimental conditions (Fig. 1C and D). We therefore used DOX-treated single-TG littermates as controls in this study.

Akt activation in lung epithelial cells *in utero* results in transient tachypnea associated with delayed maturation of the lung. Activation of Akt signaling in the lung was achieved by DOX treatment of dams starting at embryonic day 0.5 (E0.5). When analyzed at P0, DTG pups were viable and exhibited no cyanosis or growth retardation (Fig. 2A). Postnatal growth of DTG animals was also comparable to that of control mice. However, DTG mice at P0 exhibited significant tachypnea (Fig. 2B) and various histological abnormalities such as markedly reduced aerated space, increased atelectasis, bronchiolar hyperplasia, impaired thinning of the alveolar septa, and abundant PAS-positive glycogen stores (Fig. 2C to E). Since PAS-positive glycogen is normally converted to surfactant phospholipids in mature epithelial cells, these observations suggest that the differentiation of lung epithelial cells is impaired by aberrant activation of Akt signaling. Of note, these histological findings were improved spontaneously at P2 (Fig. 2C to E). Although mild elastic fiber deposition was observed at P2, no such pathology was evident at the age of 12 weeks (data not shown). Thus, Akt activation in lung epithelium induces transient respiratory difficulties associated with lung maturational defects, which improves spontaneously after birth.

Akt activation in lung epithelial cells *in utero* results in increased numbers of CC10/SP-C double-positive cells and defective maturation of lung epithelial cells. In order to further assess the extent of epithelial differentiation, we performed Western bolt analysis of surfactant proteins (SP-A to SP-D) and immunohistochemistry of marker proteins: SP-C for type II alveolar epithelial cells, Clara cell 10-kDa protein (CC10) for Clara cells, aquaporin-5 (AQP5) for type I alveolar epithelial cells, and calcitonin gene-related peptide (CGRP) for neuroendocrine cells. Western blot analysis of surfactant proteins revealed downregulation of SP-B and upregulation of

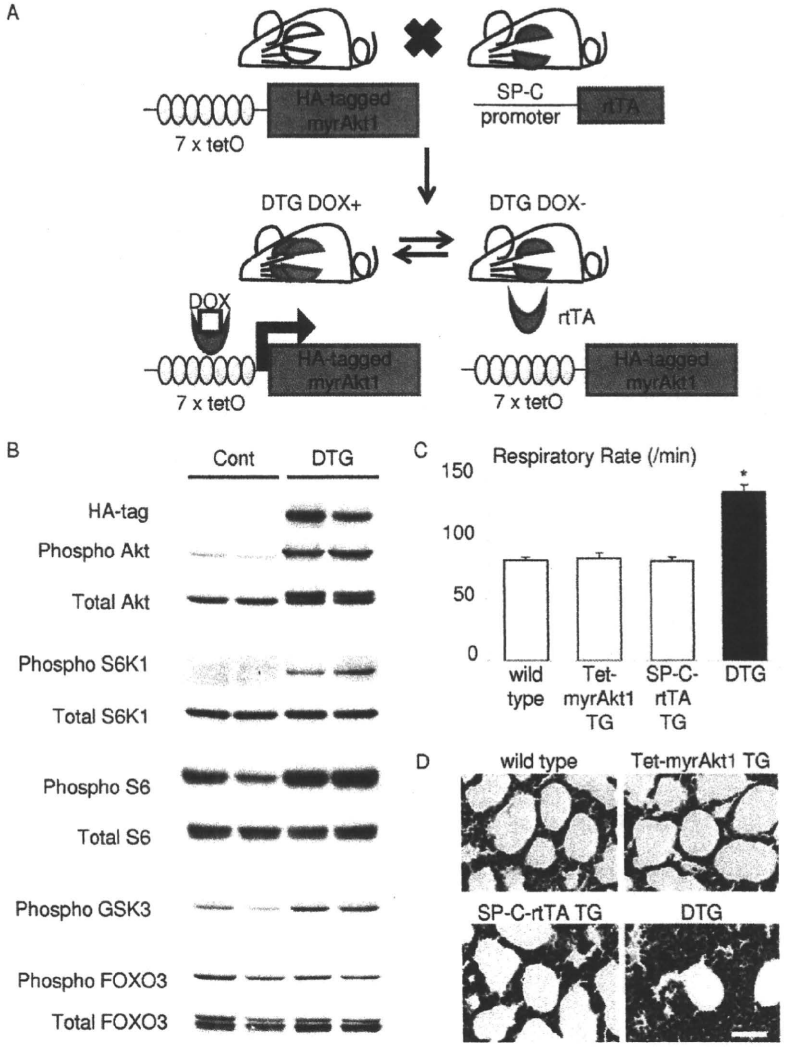

FIG. 1. Generation of bronchoalveolar epithelium-specific Akt1 TG mice. (A) Schematic illustration of binary TG system. (B) Western blot analysis of the whole-lung lysate from control and DTG mice at P0. (C) Respiratory rate at P0. DOX-treated SP-C-rtTA TG mice do not show respiratory distress. *, $P < 0.05$ versus DOX-treated wild-type, Tet-myrAkt1 TG mice, and SP-C-rtTA TG mice (n = 7, 5, 6, and 6 mice, respectively, from 3 dams). All animals were treated with DOX in the drinking water. (D) HE staining of the lung sections. Scale bar, 50 μm.

SP-D, whereas the expression levels of SP-A and SP-C were not altered (Fig. 3A). Western blot analysis and immunohistochemistry also revealed increased expression of CC10 and reduced expression of AQP5 in the lung of DTG mice (Fig. 3A and B). CGRP expression was not altered between control and DTG mice (date not shown). Previous studies characterized CC10/SP-C double-positive cells as BASCs that reside at the bronchoalveolar duct junction and differentiate to both Clara cells and type II alveolar epithelial cells; the latter further differentiate to type I alveolar epithelial cells (15). Double immunostaining revealed that CC10/SP-C double-positive cells were increased in number in the lung of DTG mice (Fig. 3C and D). Collectively, these findings suggest that aberrant activation of Akt signaling in lung epithelial cells results in increased numbers of CC10/SP-C double-positive cells and impaired differentiation of alveolar epithelial cells.

Akt activation in lung epithelial cells *in utero* results in RDS in preterm infants. Since RDS is more frequent in preterm infants than in full-term infants, we examined preterm infants born by Caesarean section at E18.5. DTG mice born at E18.5 showed cyanosis (Fig. 4A) associated with an irregular respiratory pattern, and all DTG mice died by 2 h after birth (Fig. 4B). The airway spaces of DTG lungs were filled with amorphous, proteinaceous material that was not observed in control lungs (Fig. 4C). PAS staining revealed that the size and the density of saccules in DTG lung were smaller and higher than those of controls, respectively (Fig. 4D to F). Western blot analysis of surfactant proteins revealed downregulation of SP-B, whereas the expression levels of SP-A, -C, and -D were not altered (Fig. 4G). Immunohistochemistry also revealed expansion of CC10/SP-C double-positive cells in the lung of DTG mice (Fig. 4H to J). AQP5 expression was barely detect-

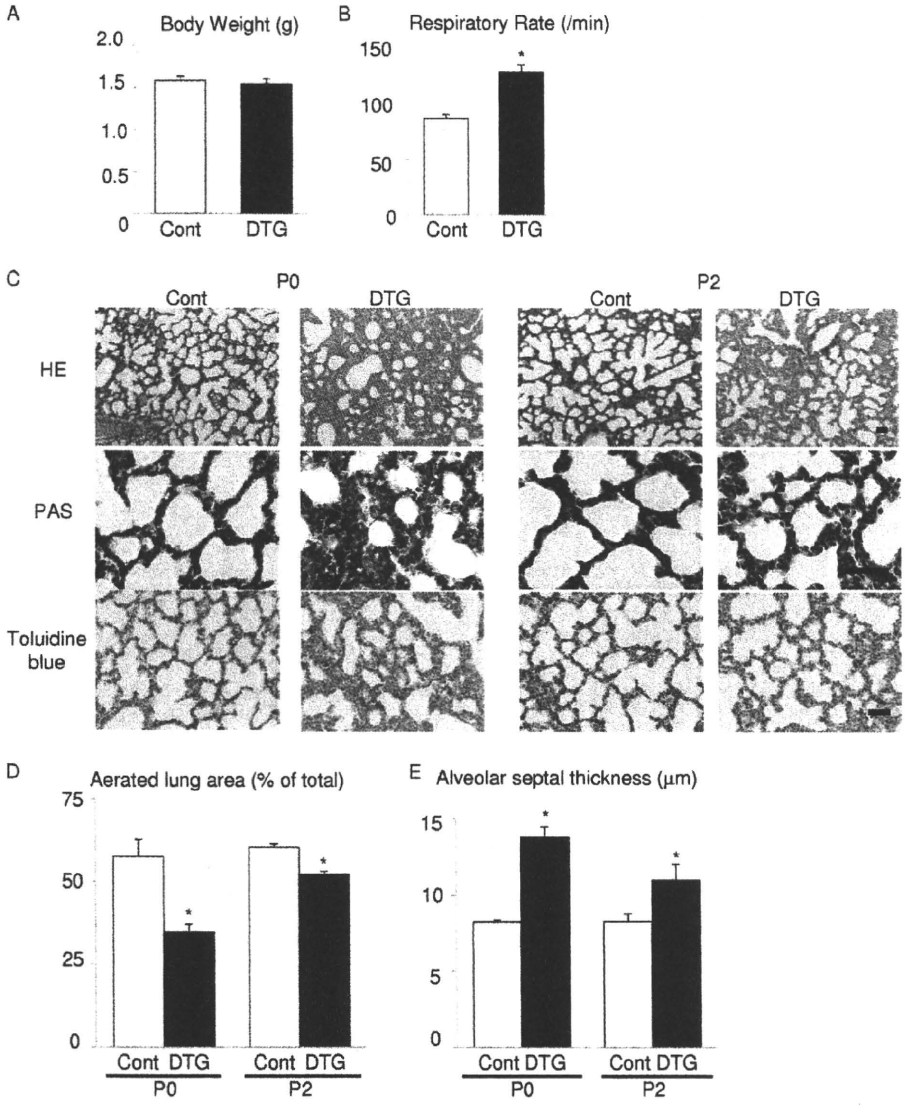

FIG. 2. Akt activation in lung epithelium induces tachypnea and delayed maturation of the lung. (A) Body weight at P0 of control (Cont; n = 6) and DTG (n = 4) mice from 2 dams. (B) Respiratory rate at P0 of control (n = 14) and DTG (n = 8) mice from 4 dams. (C) Histological analysis. HE, PAS, and toluidine blue staining of lung sections at P0 and P2. Scale bar, 50 mm. (D) Aerated lung area in control and DTG mice at P0 and P2. *, $P < 0.05$ versus control. (E) Thickness of alveolar septum in control and DTG mice at P0 and P2. *, $P < 0.05$ versus control. For experiments shown in panels D and E, n = 3 from a single dam under all conditions.

able at this stage (data not shown). These results collectively suggest that Akt activation in lung epithelial cells *in utero* results in RDS and perinatal lethality in preterm infants.

Rapamycin improves respiratory distress and lung maturational defects induced by Akt1 overexpression in lung epithelium. To test whether the Akt-mTOR pathway mediates lung pathology in DTG mice, rapamycin was administered to dams for 3 days (at E17.5, E18.5, and E19.5). Downregulation of mTOR signaling by rapamycin was confirmed by reduced phosphorylation levels of S6K1 (Fig. 5A). Examination of infants at P0 demonstrated that tachypnea observed in vehicle-treated DTG mice was improved by rapamycin treatment (Fig. 5B). Hematoxylin and eosin (HE) staining revealed that abnormal morphology of lung alveoli in DTG mice was reversed by rapamycin treatment (Fig. 5C, upper panel), and PAS staining demonstrated a reduced number of PAS-positive glycogen stores following rapamycin treatment (Fig. 5C, lower panel). By quantitative analysis of toluidine blue-stained sections, a decrease in aerated space and an increase in alveolar septal thickness observed in DTG mice were rescued by rapamycin treatment (Fig. 5D and E). Impaired differentiation of lung epithelial cells in DTG mice was also improved by rapamycin treatment, as evidenced by reduced expression of CC10, increased expression of AQP5, and a normal expression pattern of SP-C (Fig. 5F). These results suggest that mTOR is critically involved

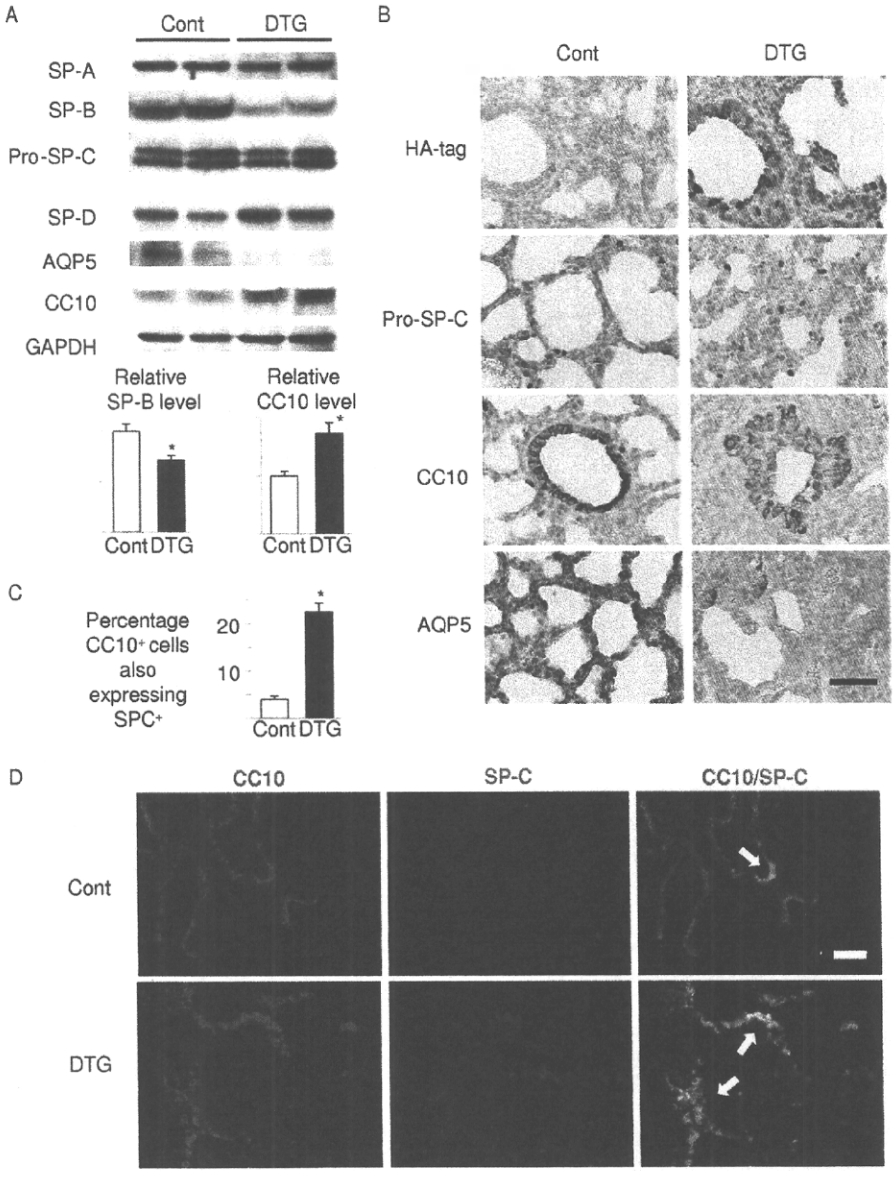

FIG. 3. Akt activation in lung epithelium results in defective maturation of lung epithelial cells and expansion of CC10/SP-C double-positive cells. (A) Western blot analysis of surfactant proteins (SP-A, SP-B, pro-SP-C, and SP-D), CC10 (a marker of Clara cells), and AQP5 (a marker of type I alveolar cells). Lower panels show densitometric analysis. *, $P < 0.05$ versus control ($n = 4$ mice from 2 dams for both controls and DTG). (B) Immunohistochemical analysis of HA tag (Akt1 transgene), SP-C, CC10, and AQP5. SP-C, CC10, and AQP5 were detected in cuboidal type II alveolar cells, Clara cells, and flat type I alveolar cells, respectively. Scale bar, 50 μm. (C and D). Double immunostaining of CC10 and SP-C. CC10/SP-C double-positive cells are indicated by arrows. Scale bar, 100 μm. *, $P < 0.05$ versus control ($n = 5$ control and $n = 3$ DTG mice from 3 dams).

in respiratory distress and lung maturational defects induced by Akt1 overexpression in lung epithelium.

Rapamycin improves respiratory distress induced by preterm delivery. The above-mentioned results suggest the possibility that mTOR activation mediates RDS in wild-type infants delivered preterm. To test this hypothesis, pregnant wild-type mice were treated with vehicle or rapamycin at E15.5 and E16.5, and pups were collected at E17.5 by Caesarean section. Inhibition of mTOR in the lung of rapamycin-treated pups was confirmed by reduced phosphorylation levels of S6K1 (Fig. 6A). All pups delivered from vehicle-treated dams died within 1 h after birth, whereas more than 50% of pups delivered from rapamycin-treated dams survived in this time frame (Fig. 6B). Histological examination revealed that rapamycin treatment promoted lung maturation, as demonstrated by increased aerated lung area, decreased alveolar septal wall thickness, a normal expression pattern of SP-C, and increased expression of AQP5 (Fig. 6C to F). Thus, downregulation of mTOR signal-

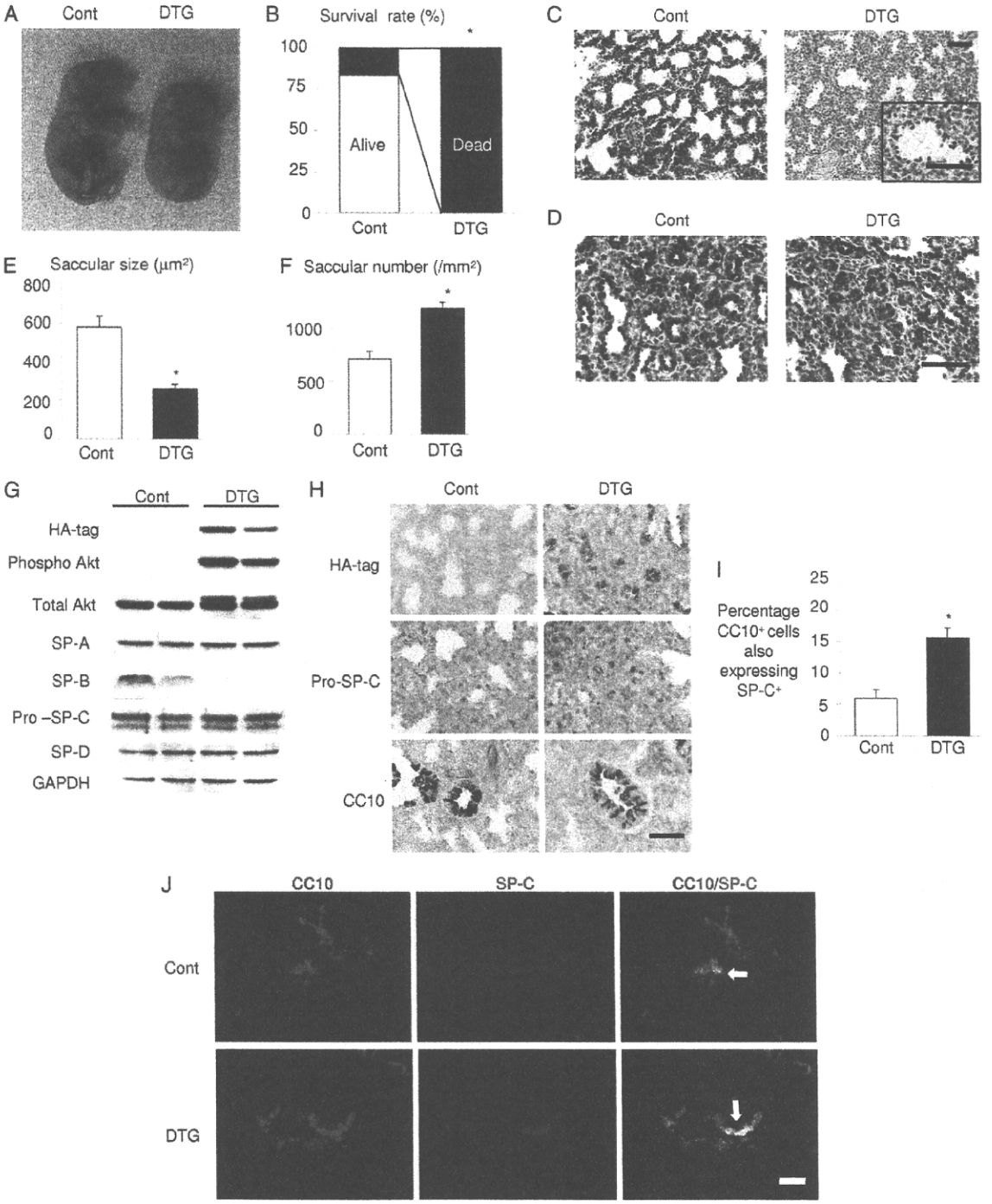

FIG. 4. Akt activation in lung epithelium results in RDS and lethality in preterm infants. (A) Gross appearance of infants. (B) Survival rate by 2 h after delivery. *, $P < 0.05$ ($n = 6$ control and $n = 5$ DTG mice from 2 dams). (C) HE staining of the lung sections of infants delivered by Caesarean section at E18.5. Scale bar, 50 μm. (D) PAS staining of the lung sections of infants delivered by Caesarean section at E18.5. Scale bar, 50 μm. (E) Saccular size at E18.5. *, $P < 0.05$ versus control. (F) Saccular number at E18.5. *, $P < 0.05$ versus control. For the experiments shown in panels E and F, $n = 3$ control and $n = 4$ DTG mice from 2 dams. (G) Western blot analysis of surfactant proteins (SP-A, SP-B, pro-SP-C, and SP-D). (H) Immunohistochemistry of HA tag (Akt1 transgene), pro-SP-C, and CC10 at E18.5. Scale bar, 50 μm. (I and J) Double immunostaining of CC10 and SP-C. CC10/SP-C double-positive cells are indicated by arrows. Scale bar, 100 μm. For both panels, $n = 4$ (Cont) and $n = 3$ (DTG) from 2 dams.

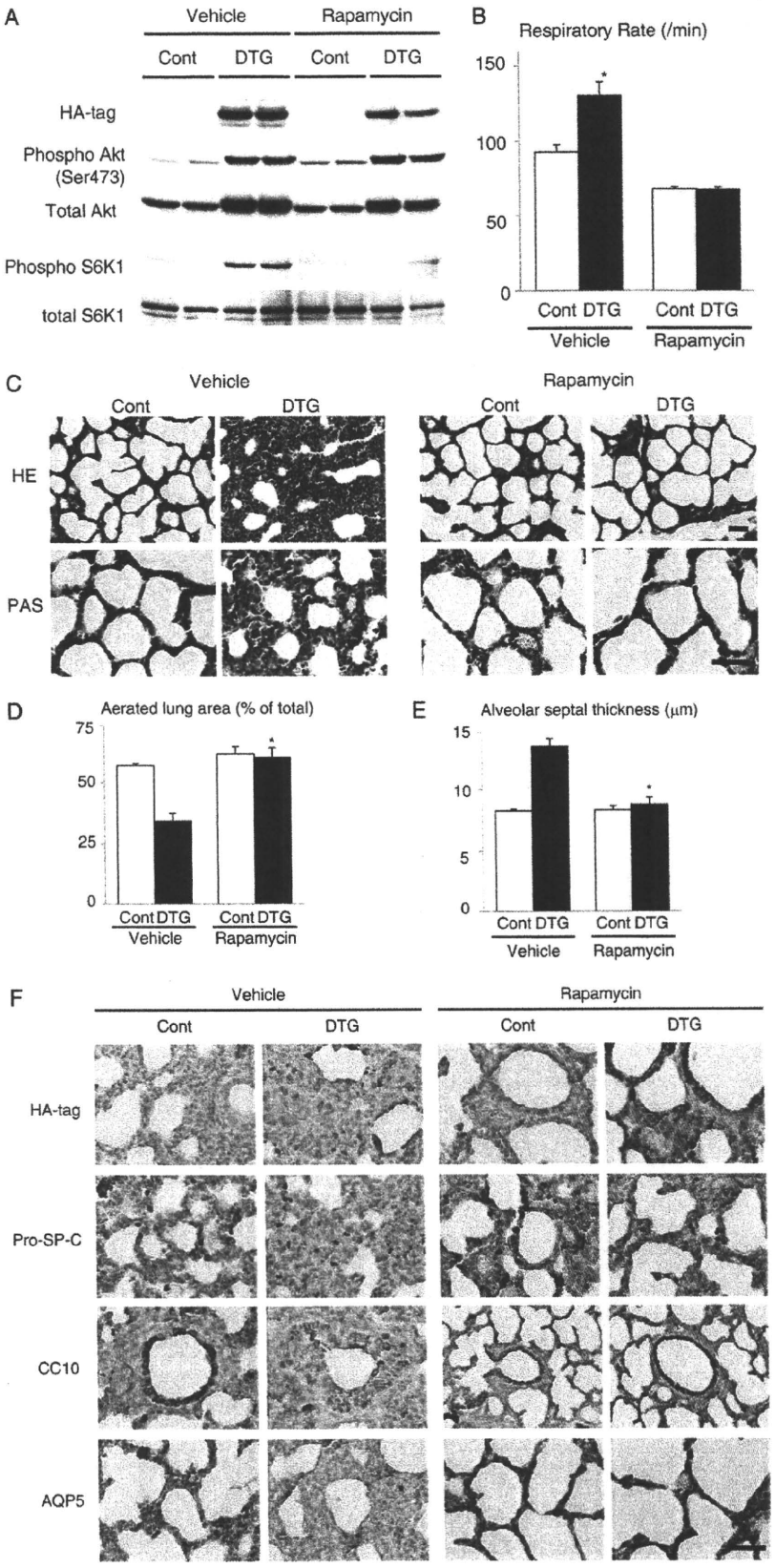
A
Vehicle
Rapamycin
Cont
DTG
Cont
DTG
HA-tag
Phospho Akt (Ser473)
Total Akt
Phospho S6K1
total S6K1
B
Respiratory Rate (/min)
150
100
50
0
Cont DTG
Cont DTG
Vehicle
Rapamycin
C
Vehicle
Rapamycin
Cont
DTG
Cont
DTG
HE
PAS
D
Aerated lung area (% of total)
75
50
25
0
Cont DTG
Cont DTG
Vehicle
Rapamycin
E
Alveolar septal thickness (μm)
15
10
5
0
Cont DTG
Cont DTG
Vehicle
Rapamycin
F
Vehicle
Rapamycin
Cont
DTG
Cont
DTG
HA-tag
Pro-SP-C
CC10
AQP5

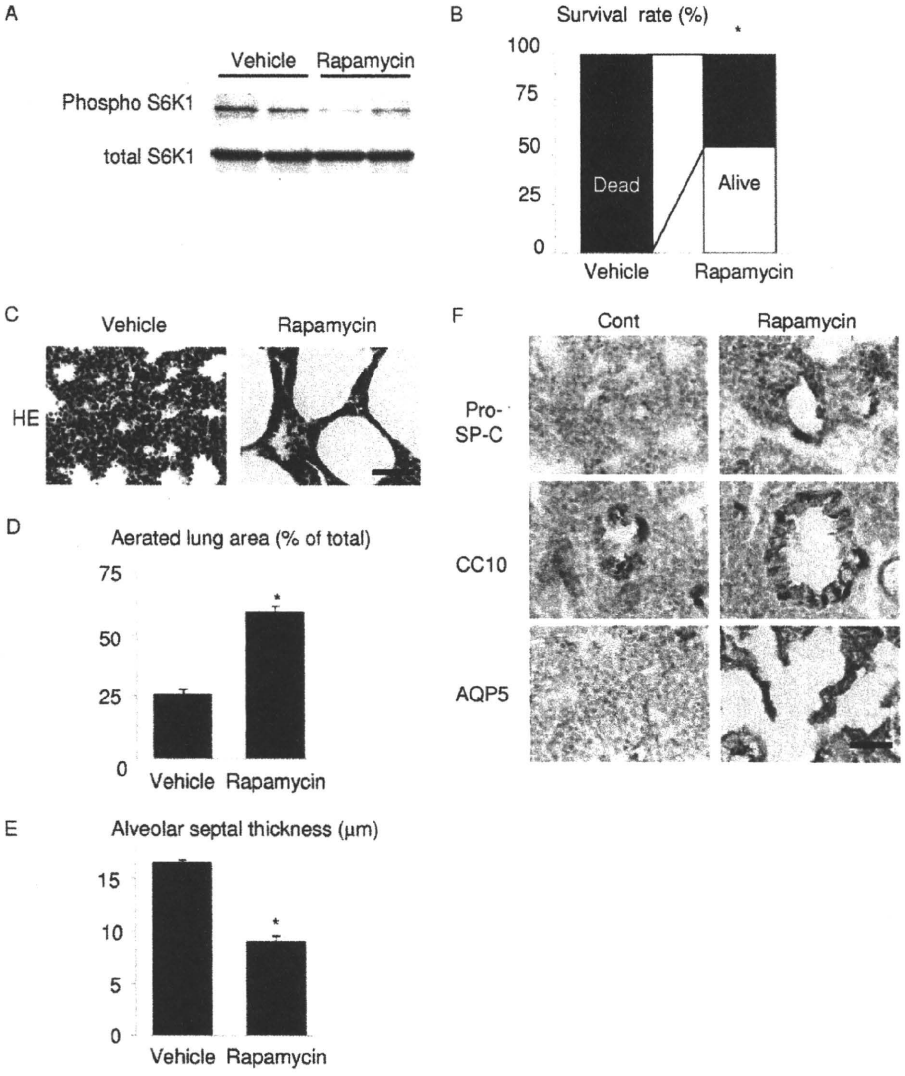

FIG. 6. Rapamycin improves respiratory distress and lung maturational defects induced by preterm delivery. (A) Western blot analysis of S6K1 in the lung. (B) Survival rate of wild-type pups 1 h after Caesarean section at E17.5. *, $P < 0.05$ versus vehicle-treated group. In the vehicle-treated group, $n = 15$ from a single dam. In the rapamycin group, $n = 24$ from 2 dams. (C) HE staining at 1 h after delivery. Scale bar, 50 μm. (D) Aerated lung area in vehicle- or rapamycin-treated pups. *, $P < 0.05$ versus vehicle-treated group. In the vehicle-treated group, $n = 3$ from a single dam; in the rapamycin group, $n = 4$ from 2 dams. (E) Thickness of alveolar septum in vehicle- or rapamycin-treated pups. *, $P < 0.05$ versus vehicle-treated group. In the vehicle-treated group, $n = 3$ from a single dam; in the rapamycin group, $n = 4$ from 2 dams. (F) Immunohistochemistry of pro-SP-C, CC10, and AQP5. Scale bar, 50 μm.

ing has a therapeutic potential for RDS induced by preterm delivery in wild-type mice.

Activation of the Akt-mTOR pathway attenuates HIF-2-dependent VEGF expression in lung epithelial cells. To investigate the mechanism by which Akt-mTOR signaling affects lung maturation, we examined the expression of VEGF, an angiogenic growth factor that is produced in the distal airway during late gestation and regulates coordinated development of alve-

FIG. 5. Rapamycin improves respiratory distress and lung maturational defects induced by Akt1 overexpression in lung epithelium. (A) Western blot analysis of Akt and S6K1 in the lung. (B) Respiratory rate of vehicle- or rapamycin-treated pups at P0. For vehicle experiments, $n = 7$ for both control and DTG mice from 3 dams; for rapamycin experiments, $n = 14$ (control) and $n = 11$ (DTG) mice from 4 dams. (C) Histological analysis. HE and PAS staining of lung sections at P0. Scale bar, 50 μm. (D) Aerated lung area in vehicle- or rapamycin-treated pups at P0. *, $P < 0.05$ versus vehicle-treated DTG mice. (E) Thickness of alveolar septum in vehicle- or rapamycin-treated pups at P0. *, $P < 0.05$ versus vehicle-treated DTG mice. For experiments shown in panels D and E, $n = 3$ control and $n = 3$ DTG vehicle-treated mice from 3 dams, and $n = 8$ control and $n = 7$ DTG rapamycin-treated mice from 4 dams. (F) Immunohistochemistry of HA tag, pro-SP-C, CC10, and AQP5 at P0. Scale bar, 50 μm.

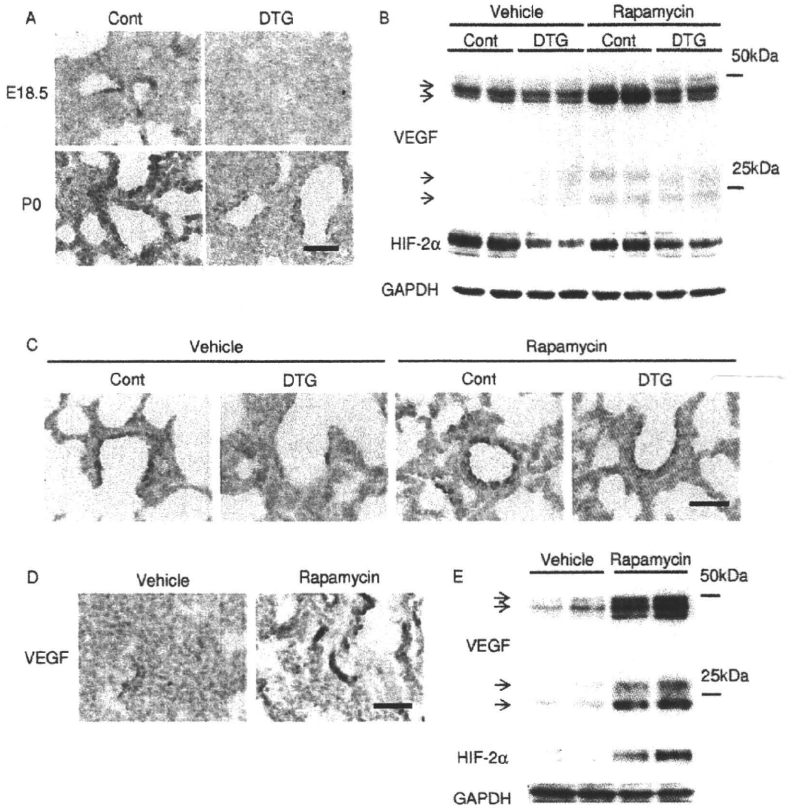

FIG. 7. Akt-mTOR pathway downregulates VEGF expression in the lung. (A) Immunostaining of VEGF at E18.5 and P0 in Akt1 TG mice. Scale bar, 50 μm. (B) Western blot analysis of VEGF and HIF-2α at P0 in Akt1 TG mice. (C) Immunostaining of VEGF at P0 in Akt1 TG mice. Scale bar, 50 μm. (D) Immunostaining of VEGF at E17.5 in wild-type mice. Scale bar, 50 μm. (E) Western blot analysis of VEGF and HIF-2α at E17.5 in wild-type mice.

olar epithelium and capillaries (4). Immunohistochemistry and Western blot analysis revealed that the expression levels of VEGF were downregulated in DTG mice both at E18.5 and P0 and were restored by rapamycin treatment (Fig. 7A to C). Since the expression of VEGF in the lung has been reported to depend on HIF-2 activity (4), we next examined the expression of HIF-2α protein in the lung. Western blot analysis revealed that the HIF-2α protein amount was downregulated in the lung of DTG mice (Fig. 7B). The expression levels of VEGF and HIF-2α were also examined in vehicle- or rapamycin-treated wild-type pups delivered at E17.5. Immunohistochemistry and Western blot analysis demonstrated the upregulation of VEGF and HIF-2α expression by rapamycin in wild-type mice delivered preterm (Fig. 7D and E). It was therefore concluded that activation of the Akt-mTOR pathway attenuates the expressions of VEGF and HIF-2α in the lung. However, it was also noted that the expression levels of HIF-2α do not necessarily correlate with those of VEGF because rapamycin treatment highly upregulated VEGF expression in control animals without altering HIF-2α expression levels (Fig. 7B, compare the vehicle control group and the rapamycin control group). We therefore examined whether Akt-mTOR signaling regulates the transcriptional activity of HIF-2. In cultured A549 lung epithelial cells, insulin induced downregulation of VEGF expression, which was reversed by rapamycin treatment (Fig. 8A). Luciferase assays using *VEGF-luc* as a reporter gene revealed that insulin attenuated transcriptional activity of HIF-2 on VEGF promoter, which was reversed by rapamycin treatment (Fig. 8B), while both insulin and rapamycin had minimal effects on HIF-1 transcriptional activity (Fig. 8C). These results suggest that activation of Akt-mTOR signaling attenuates HIF-2-dependent VEGF expression with respect to both the amount of HIF-2α protein and HIF-2 transcriptional activity.

Activation of the Akt-mTOR pathway reduces alveolar capillary density. To test whether Akt-mTOR-mediated downregulation of VEGF is associated with attenuated alveolar angiogenesis, vascular morphometry was performed in DTG and control mice at P0. Isolectin B4 staining revealed that alveolar capillary density was significantly reduced in DTG mice compared to that in control mice, and this reduction was rescued by rapamycin treatment (Fig. 9A and B). We also found that alveolar capillary density in wild-type mice delivered preterm at E17.5 was increased by rapamycin treatment (Fig. 9C and D). Thus, alveolar capillary density is closely linked to the level of VEGF expression in the lung. These results are consistent with our hypothesis that Akt-mTOR signaling promotes RDS through downregulation of VEGF.

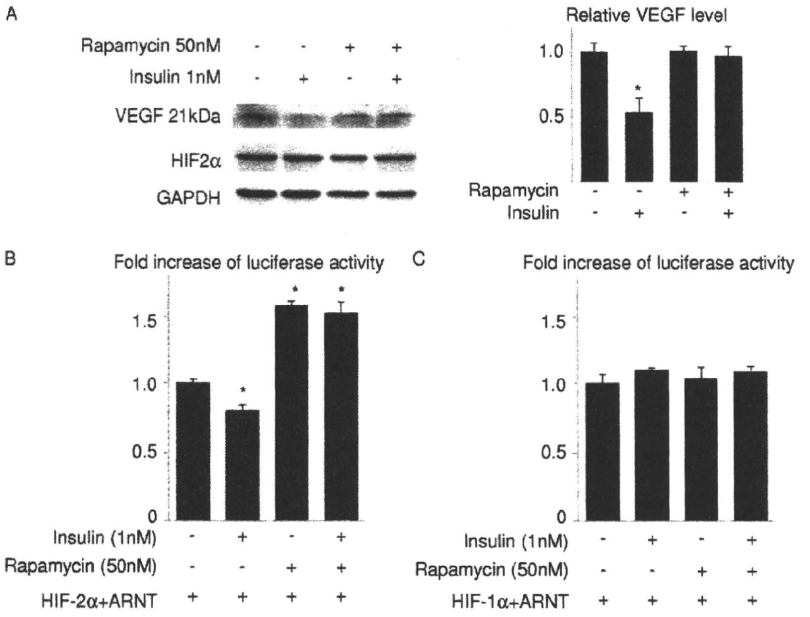

FIG. 8. Insulin attenuates VEGF expression and HIF-2 transcriptional activity on *VEGF* promoter in an mTOR-dependent manner in lung epithelial cells. (A) Western blot analysis of VEGF and HIF-2α in A549 cells treated with insulin and/or rapamycin for 48 h. The right panel shows the densitometric analysis. *, $P < 0.05$ versus the rapamycin (−)/insulin (−) group ($n = 3$ for each group). (B and C) Luciferase assays in A549 cells. A549 cells were transfected with a *VEGF-luc* reporter and expression vectors for HIF-1α, HIF-2α, and ARNT and treated with insulin and/or rapamycin. All experiments were performed in the presence of $CoCl_2$ to mimic hypoxic conditions. *, $P < 0.05$ versus the rapamycin (−)/insulin (−) group.

DISCUSSION

In this study we have demonstrated that activation of Akt signaling in lung epithelial cells during embryogenesis results in transient respiratory difficulties in full-term infants and in RDS in preterm infants. These respiratory defects were associated with bronchiolar hyperplasia, expansion of CC10/SP-C double-positive cells, and impaired maturation of lung epithelial cells. We also found that Akt-mTOR signaling is critically involved in the pathogenesis of RDS because rapamycin treatment improved respiratory distress and lung maturational defects induced by Akt activation or preterm delivery. Mechanistically, Akt-mTOR signaling attenuates both the protein amounts and transcriptional activity of HIF-2, leading to downregulation of HIF-2-dependent expression of VEGF, an angiogenic growth factor that is required for maturation of alveolar epithelial cells. These observations suggest the possibility that aberrant activation of Akt-mTOR signaling or preterm delivery before the appropriate downregulation of this signaling axis plays a causal role in RDS through downregulation of HIF-2-dependent VEGF expression and that the mTOR-HIF-2 pathway may be a novel therapeutic target for infant RDS.

RDS is frequently observed in infants of diabetic mothers, and hyperactivation of insulin signaling in response to maternal hyperglycemia has been proposed to play a pathogenic role (19, 22). It was also previously shown that alveolar epithelium-specific deletion of *Pten* results in RDS, with approximately 90% of neonates dying within 2 h after birth (33). This phenotype of conditional *Pten* deletion is more severe than that of alveolar epithelium-specific Akt1 transgenic mice, suggesting the possibility that PI3K-dependent but Akt-independent pathways are also implicated in the occurrence of RDS. However, because another line of lung epithelium-specific *Pten* knockout mice generated by a similar method exhibit a very mild phenotype (i.e., lack of neonatal lethality, normal postnatal development, and mild bronchiolar hyperplasia) (7), the variation of phenotypes among different animal models may be due in part to the differences in the genetic background of the animals. Furthermore, rapamycin treatment of dams significantly improved the phenotype of alveolar epithelium-specific Akt1 transgenic mice. Taken together, these observations suggest that activation of the PI3K-Akt-mTOR pathway in lung epithelial cells *in utero* plays a causal role in the pathogenesis of RDS in infants with diabetic mothers.

Lung development in mice is histologically divided into four phases: the pseudoglandular stage (E9.5 to 16.5), canalicular stage (E16.5 to 17.5), terminal sac stage (E17.5 to P5), and alveolar stage (P5 to P30) (30). Differentiation of type I and type II epithelial cells and high levels of Pten expression in respiratory epithelium occur at the terminal sac stage (17), which is consistent with the idea that downregulation of the PI3K-Akt-mTOR pathway is required for epithelial differentiation. In humans, lung development is relatively advanced compared with that of mice, and the terminal sac stage corresponds to human preterm infants between 26 and 36 weeks of gestation, when a high complication rate of RDS is observed. Thus, inhibition of the PI3K-Akt-mTOR pathway at specific time points during a later stage of embryogenesis appears to be critical for normal lung development and maturation, and aberrant activation of Akt-mTOR signaling or preterm delivery

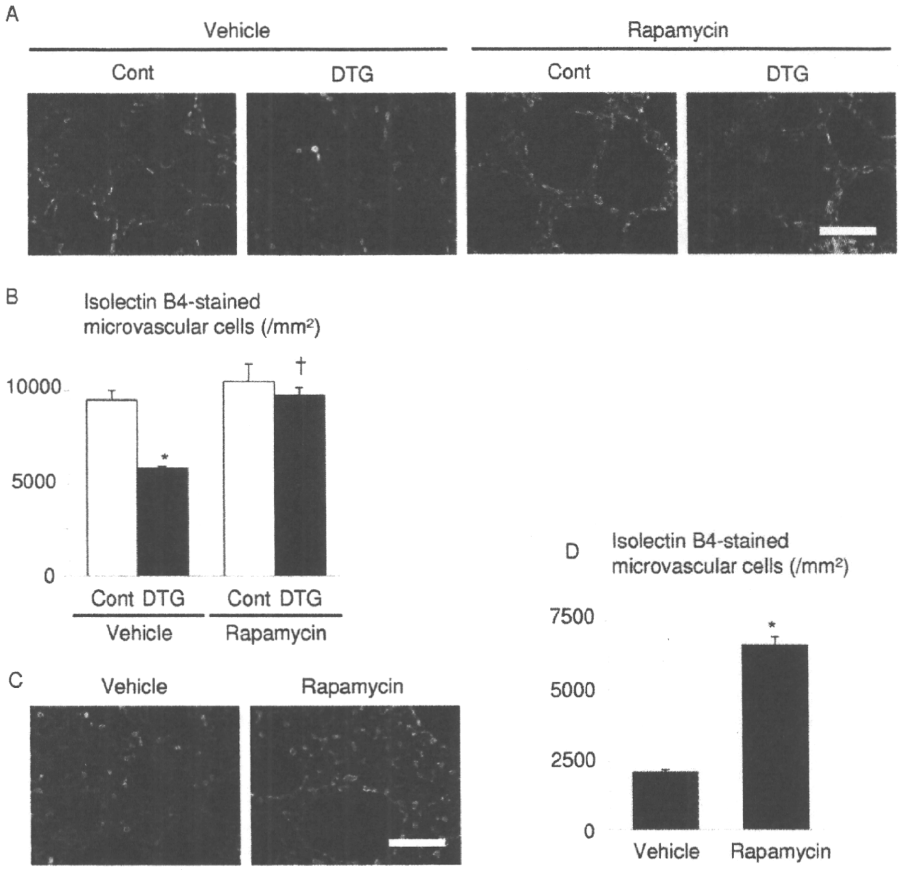

FIG. 9. Alveolar capillary bed formation is impaired by Akt1 overexpression in lung epithelium, which is improved by rapamycin administration to the dams. (A) Histological analysis of vehicle- or rapamycin-treated pups at P0. Sections were stained with isolectin B4-FITC conjugate (green) to detect endothelial cells and with wheat germ agglutinin-TRITC conjugate (red) for membrane staining. Scale bar, 50 μm. (B) Alveolar capillary density. *, $P < 0.05$ versus vehicle-treated control mice; †, $P < 0.05$ versus vehicle-treated DTG mice. In the vehicle-treated group, $n = 4$ control and $n = 3$ DTG mice from 2 dams; in the rapamycin group, $n = 4$ control and $n = 4$ DTG mice from 2 dams. (C) Histological analysis of vehicle- or rapamycin-treated wild-type pups born by Caesarean section at E17.5. Scale bar, 50 μm. (D) Alveolar capillary density. *, $P < 0.05$ versus vehicle-treated mice ($n = 4$ vehicle-treated mice from a single dam, and $n = 4$ rapamycin-treated mice from 2 dams).

before this signaling pathway is appropriately downregulated may result in the occurrence of RDS. The observation that rapamycin was effective for RDS also suggests that downregulation of mTOR signaling is sufficient to induce maturation of lung epithelial cells. Previous studies also implicated GATA6-Wnt/β-catenin signaling and calcineurin/nuclear factor of activated T cells (NFAT) signaling in lung maturation (6, 34). How these two signaling pathways and the PI3K-Akt-mTOR pathway coordinately regulate normal lung development remains to be investigated. It should also be noted that VEGF-induced angiogenesis is enhanced in the presence of rapamycin, which is inconsistent with the observation that VEGF induces endothelial cell proliferation via the Akt-mTOR pathway (32). This may be in part explained by the proangiogenic effects of the rapamycin-insensitive downstream effectors of Akt such as glycogen synthase kinase-3 and the FOXO family of transcription factors (1, 16).

Epithelial-endothelial interactions during lung development are critical in establishing a functional blood-gas interface, and normal lung function depends on the coordinated development of alveolar epithelium and capillaries, which is primarily regulated by VEGF (27). It was previously shown that deletion of HIF-2α in mice causes RDS due to downregulation of HIF-2-dependent VEGF expression in the lung (4). The similarity of the phenotypes between lung epithelium-specific Akt1 TG mice and HIF-2α-deficient mice prompted us to investigate the mechanistic link between mTOR and HIF-2. Previous studies showed that mTOR enhances the transcriptional activity of HIF-1 (13) and that VEGF expression in the heart is induced by activation of the Akt-mTOR pathway in TG mice in which the Akt1 transgene is inducible in the heart by doxycycline treatment (25), suggesting that mTOR promotes HIF-1-dependent VEGF expression. However, VEGF expression in the lung was downregulated by Akt1 overexpression and restored by rapamycin treatment. Consistently, HIF-2α expression levels were downregulated in the lung of DTG mice, and reporter gene assays in cultured lung epithelial cells revealed that insulin attenuates the transcriptional activity of HIF-2 on VEGF promoter in an mTOR-dependent manner. These results suggest the possibility that HIF-2 and VEGF are situated down-